https://doi.org/10.5194/acp-2019-905
Preprint. Discussion started: 14 October 2019

Atmospheric Chemistry and Physics Discussions
Open Access EGU

Impact of topography on black carbon transport to the southern Tibetan Plateau during pre-monsoon season and its climatic implication

[1]Meixin Zhang, [1]Chun Zhao*, [2,3]Zhiyuan Cong, [1]Qiuyan Du, [1]Mingyue Xu, [1]Yu Chen, [4]Ming Chen, [1]Rui Li, [1]Yunfei Fu, [1]Lei Zhong, [3,5]Shichang Kang, [6]Delong Zhao, [6]Yan Yang

[1]School of Earth and Space Sciences, University of Science and Technology of China, Hefei, China
[2]Key Laboratory of Tibetan Environment Changes and Land Surface Processes, Institute of Tibetan Plateau Research, Chinese Academy of Sciences (CAS), Beijing 100101, China
[3]CAS Center for Excellence in Tibetan Plateau Earth Sciences, Institute of Tibetan Plateau Research, CAS, Beijing 100101, China
[4]National Center for Atmospheric Research, Boulder, CO, USA
[5]State Key Laboratory of Cryosphere Science, Northwest Institute of Eco-Environment and Resources, CAS, Lanzhou 730000, China
[6]Beijing Weather Modification Office, Beijing 100101, China

Manuscript for submission to Atmos. Chem. Phys.

*Corresponding author: Chun Zhao (chunzhao@ustc.edu.cn)

Key points:
1. The simulations show evident accumulation of aerosols near the southern Himalayas during the pre-monsoon season.
2. The prevailing up-flow across the Himalayas driven by the large-scale circulation during the daytime is the dominant mechanism of South Asian BC transport to the TP.
3. The BC transport across the Himalayas can overcome the mountain ridges, but the valley transport is much more efficient.
4. The simulation at 4 km resolution generates 50% higher transport flux of BC across the Himalayas and 30-40% stronger BC radiative heating in the atmosphere over the TP than that at 20 km resolution, primarily due to their different representations of topography, which implies that global climate models with relatively coarse resolution may introduce significant negative biases in estimating BC radiative forcing over the TP.

https://doi.org/10.5194/acp-2019-905
Preprint. Discussion started: 14 October 2019

Atmospheric Chemistry and Physics Discussions

Abstract

Most of previous modeling studies about black carbon (BC) transport and impact over the Tibetan Plateau conducted simulations with horizontal resolutions coarser than 10 km that may not be able to resolve well the complex topography of the Himalayas. In this study, the experiments with WRF-Chem at two horizontal resolutions (20 km and 4 km) are conducted for pre-monsoon season (April, 2016) to investigate the impacts of topography on modeling the transport and distribution of BC over the TP. The simulations at both resolutions show evident accumulation of aerosols near the southern Himalayas during the pre-monsoon season, consistent with the satellite retrievals. The observed episode of high surface BC concentrations at the station near the Mt. Everest due to heavy biomass burning near the TP is well captured by the simulations. The simulations at both resolutions indicate that the prevailing up-flow across the Himalayas driven by the large-scale circulation during the daytime is the dominant transport mechanism of South Asian BC into the TP, and is much stronger than that during the nighttime. The valley wind can strengthen the prevailing up-flow transport. The simulations at coarse resolution (20 km) and fine resolution (4 km) show large differences in representing the distributions of topography of the Himalayas. The simulation at 4 km resolution resolves more valleys and thus produces much stronger transport fluxes, which indicates that although the transport of South Asian BC across the Himalayas can overcome the mountain ridges, the valley transport is more efficient and cannot be ignored. This results in 50% higher transport flux of BC across the Himalayas and 30-40% stronger BC radiative heating in the atmosphere over the TP from the simulation at 4 km than that at 20 km resolution. The different topography also leads to different distributions of snow cover and BC forcing in snow. This study implies that global climate models generally with even coarser resolutions than 20 km may introduce significant negative biases in estimating light absorbing aerosol radiative forcing over the TP.

https://doi.org/10.5194/acp-2019-905
Preprint. Discussion started: 14 October 2019

Atmospheric Chemistry and Physics Discussions

1. Introduction

The Tibetan Plateau (TP) is the highest plateau in the world with an average elevation over 4 km and an area of approximately 2.5 × 10^6 km^2, known as the world's third pole (Qiu, 2008), and its enormous dynamic and thermal effects have a huge impact on large-scale atmospheric circulation, such as Asian monsoon, and environmental changes through the energy exchange with free atmosphere (e.g., Ye and Wu,1998; Duan and Wu, 2005; Wu et al., 2005, 2012, 2019; Boos and Kuang, 2013; Chen and Bordoni, 2014; He et al., 2019; Zhao et al., 2019). The increase in aerosol concentration in the atmosphere over/around the TP can change the circulation pattern over Asia (e.g., Qian et al., 2011, 2015; Lau et al., 2016, 2017, 2018). Model simulations showed that the absorptive aerosols changed the surface radiative flux over the TP by 5-25 W m^{-2} during the pre-monsoon season in April and May and led to the changes in summer monsoon circulations (Qian et al., 2011). Meanwhile, aerosol may affect the atmosphere by modulating the vertical structure of cloud and precipitation around the TP, and thus change the distribution of atmospheric latent heat around the TP, which is the main driving force of regional atmosphere circulation (e.g., Li et al 2010, 2017, 2019). In addition, the TP is rich in glaciers and snow resources, the glacial melting water is one of the important sources of water resources of the Indus River, Ganges River, Yangtze River, and Yellow River in Asia (e.g., Singh and Bengtsson, 2004; Barnett et al., 2005; Immerzeel et al., 2010; Lutz et al., 2014). When absorbing aerosols adhere, they will blacken the surface of snow cover and glacier to a large extent (e.g., Hansen and Nazarenko., 2004; Ramanathan and Carmichael, 2008; Lau et al., 2010, 2019; Lee at al., 2013; Zhang, Y. L., 2017, 2018), and then reduce the snow albedo so as to absorb more solar radiation and cause the consequences of accelerated melting (e.g., Ramanathan et al., 2007; Ming et al., 2009; Yasunari et al., 2010; Ji et al., 2015; Zhang et al., 2015). According to the IPCC AR5, the radiative forcing caused by the important component of absorbing aerosols, black carbon (BC), on the surface snow is 0.04 W m^{-2} (0.02-0.09 W m^{-2}) on global average, and the regional forcing (such as over the Arctic and the Himalayas) can be considerably large.

The TP is surrounded by anthropogenic sources of pollutants. Over the South of TP, previous studies have suggested that South Asia are the main sources of pollutants transported over the plateau (e.g., Cong et al., 2009, 2015a,b; Kopacz et al., 2011; Lu et al., 2012; Zhao et al., 2013; Wang et al., 2015; Zhang et al., 2015; Kang et al., 2015; Li et al., 2016; Chen et al., 2018; Kang et al., 2019). A huge blanket or layer of "haze" generally composes of light-absorbing carbonaceous aerosol particles that often erupts in the

https://doi.org/10.5194/acp-2019-905
Preprint. Discussion started: 14 October 2019

Atmospheric Chemistry and Physics Discussions

pre-monsoon season over South Asia and has a significant influence on the plateau (e.g., Prasad and Singh, 2007; Engling and Gelencser, 2010). The strong biomass burning reaching the maximum in pre-monsoon season over South Asia also leads to high loading of absorbing aerosols over the southern TP (e.g., Cong et al., 2015b). Many studies investigated the transport mechanisms of South Asian pollutants to the TP and found that the pollutant transport across the Himalayas was mainly due to the combination of large-scale circulation and regional winds (e.g., Hindman and Upadhyay, 2002; Cao et al., 2010; Dumka et al., 2010; Marinoni et al., 2010; Cong et al., 2015a; Kang et al., 2015; Luthi et al., 2015; Zhang et al., 2017). Cong et al. (2015a) conducted seven-day backward air-mass trajectories experiment and found strong westerlies pass through western Nepal, northwest India and Pakistan (i.e., southern Himalayas) in the pre-monsoon season. Dumka et al. (2010) and Kang et al. (2015) inferred from the trajectory analysis that long-distance transport from Africa and Europe may also affect the BC concentration of Himalayas in addition to the influence of regional pollution. Zhang et al. (2017) suggested that the cut-off low pressure in the upper and middle layers of the troposphere can enhance the transport by the westerlies to the plateau based on a chemical transport model.

Although previous studies have confirmed the transport of pollutants across the Himalayas, the complex topography of Himalayas complicates transport mechanisms. On one hand, Cao et al. (2010) revealed that the Himalayas acts as a huge barrier to the transport of a large amount of BC over the plateau based on model simulations. On the other hand, some studies found that the valleys across the Himalayas serve as channels for efficient transport of pollutants (e.g., Hindman and Upadhyay, 2002; Marinoni et al., 2010). Marinoni et al. (2010) analyzed the wind field observation at one site and found that a distinct valley wind system with the southerlies continuously transported pollutants to the plateau. Most of these studies used observations and back-trajectory models to demonstrate the transport pathways of pollutants to the TP, which cannot explicitly reveal the transport mechanisms underneath, in particular quantifying the impacts of complex topography. A few of modeling studies investigated the pollutant transport mechanisms using 3-D chemical transport models (e.g., Kopacz et al., 2011; Liu et al., 2015; Zhang et al., 2017; Yang et al., 2018). However, most of them simulated transport processes at relatively coarse horizontal resolutions (e.g., 20-100 km), which cannot resolve well the complex topography of the Himalayas. It is noteworthy that studies about the aerosol climatic impact over the TP also used climate models at relatively coarse horizontal resolutions (e.g., Flanner and Zender, 2005; Menon et al., 2010; Kopacz et al., 2011; Qian et al., 2011, 2015; He et al., 2014; Zhang et al., 2015; Ji et al.,

https://doi.org/10.5194/acp-2019-905
Preprint. Discussion started: 14 October 2019

2016). So far, there is only one study that used a chemical transport model at a horizontal resolution of sub-10 km to investigate pollutant transport mechanisms over the eastern Himalayas (Cao et al., 2010). Furthermore, none of studies assessed quantitatively the impacts of topography on modeling the pollutant transport across the Himalayas and hence on estimating aerosol distribution and radiative forcing over the TP.

This study uses the Weather Research and Forecasting Model coupled with chemistry (WRF-Chem, Grell et al., 2005; Skamarock et al., 2008) to investigate the impacts of topography on pollutant transport across the Himalayas. The experiments with two different horizontal resolutions (4 km versus 20 km) are conducted to illustrate the impacts on the transport mechanisms. The simulations are conducted for April 2016 in pre-monsoon season, because South Asia is seriously polluted during this period and the pollutants transported to the TP during the period may have significant impacts on Asian monsoon system (e.g., Lau et al., 2006a, b; Ding et al., 2009; Kuhlmann and Quaas, 2010; Qian et al., 2011, 2015). In addition, the observed concentration of BC at the observation site besides Mt. Everest showed an evident pollution episode from April 5th to 15th of 2016, deserving the investigation of the transport mechanisms. This study particularly focuses on the impacts of different topographic representations in simulations at various horizontal resolutions on pollutant transport across the Himalayas and the resulting radiative forcing.

The rest of the paper is organized as follows. Section 2 describes briefly the WRF-Chem model, the physics parameterizations, and the model configuration for this study, followed by a description of data for evaluation. The series of numerical experiments at different resolutions are analyzed in Section 3. The findings are then summarized in Section 4.

2. Methodology

2.1 Model and experiments

2.1.1 WRF-Chem model

In this study, the version of WRF-Chem updated by University of Science and Technology of China (USTC version of WRF-Chem) is used. This USTC version of WRF-Chem includes some additional capabilities such as the diagnosis of radiative forcing of aerosol species, land surface coupled biogenic VOC emission, aerosol-snow interaction compared with the publically released version (Zhao et al., 2013a,b, 2014, 2016; Hu et al., 2019). The MOSAIC (Model for Simulating Aerosol Interactions and Chemistry) aerosol model (Zaveri et al., 2008) and the CBM-Z (carbon bond mechanism) gas phase mechanisms

https://doi.org/10.5194/acp-2019-905
Preprint. Discussion started: 14 October 2019

(Zaveri and Peters, 1999) are selected. The MOSAIC aerosol scheme uses an approach of segmentation to represent aerosol size distribution with four or eight discrete size bins (Fast et al., 2006). The MOSAIC scheme classifies aerosols into multiple components including OM (organic matter), BC (black carbon), NO_3^- (nitrate), SO_4^{2-} (sulfate), NH_4^+ (ammonium), sea salt, mineral dust, and OIN (other inorganic). It consists of a range of physical and chemical processes such as nucleation, condensation, coagulation, aqueous phase chemistry, and water uptake by aerosol. The parameterization of dry deposition of aerosol mass and number is according to the method of Binkowski and Shankar (1995), including particle diffusion and gravitational effects. Aerosol-cloud interactions were included in the model by Gustafson et al. (2007) for calculating the activation and re-suspension between dry aerosols and cloud droplets. The wet removal of grid-resolved stratiform clouds/precipitation includes two aspects, namely in-cloud removal (rainout) and below-cloud removal (washout) by Easter et al. (2004) and Chapman et al. (2009), respectively. Aerosol optical properties such as single scattering albedo (SSA) and scattering asymmetry and so on are calculated at each model grid through the function of wavelength. The shortwave (SW) and longwave (LW) refractive indices of aerosols use the Optical Properties of Aerosols and Clouds (OPAC) data set (Hess et al., 1998), with a detailed description of the computation of aerosol optical properties can be found in Barnard et al. (2010) and Zhao et al. (2013a). For both short wave and long wave radiation, aerosol radiation feedback combined with Rapid Radiative Transfer Model (RRTMG) (Mlawer et al., 1997; Iacono et al., 2000) was implemented by Zhao et al (2011). For the diagnose of the optical properties and direct radiative forcing of various aerosol species in the atmosphere, adopted the method described by Zhao et al (2013a). The radiative forcing of light absorbing aerosol in surface snow is estimated with the SNICAR model (Flanner and Zender, 2005) in the land surface scheme as introduced by Zhao et al. (2014).

2.1.2 Numerical experiments

In this study, the WRF-Chem simulations are performed with two nested domains (one-way nesting), one outer domain at 20 km horizontal resolution with 350×250 grid cells (62-112°E, 0-38°N) and one inner domain at 4 km horizontal resolution with 400×300 grid cells (75-91°E, 24-35°N) (Figure 1). The inner domain roughly covers the entire Himalayas. To resolve the vertical structure of transport across the Himalayas, the simulations are configured with 54 vertical layers and roughly 17 layers below 2 km above the ground

https://doi.org/10.5194/acp-2019-905
Preprint. Discussion started: 14 October 2019

(Figure 2). The goal of this study is to investigate the different representations of topography on the transport. Figure 3 shows the spatial distribution of terrain height from the outer domain at 20 km resolution and the inter domain at 4 km over the Himalayas (75-91°E, 24-35°N). It is evident that the terrain is much smoother at 20 km than at 4 km resolution. The hillsides and valleys can be resolved to some extent at 4 km resolution but mostly missed at 20 km. The probability distributions of terrain height at 20 km and 4 km resolutions (Fig. S1 in the supporting material) show that the difference between the two resolutions is small for the terrain height lower than ~4 km but is significant for the terrain height above ~4 km. The simulations are conducted for March 29th-April 20 of 2016. The results of April 5th-20th are analyzed for the observed pollution episode.

The meteorological initial and lateral boundary conditions are derived from the ECMWF reanalysis data at 0.5°×0.66° horizontal resolution and 6 h temporal intervals. The modeled u component and v component wind and atmospheric temperature are nudged towards the reanalysis data with a nudging timescale of 6 h (Stauffer and Seaman, 1990; Seaman et al., 1995; Liu et al., 2012). Spectral nudging method is applied to balance the performance of simulation at the large and small scales (Liu et al., 2012), and only to the layers above the PBL with nudging coefficients of 3×10^{-4} s^{-1}. A wave number of three is selected for both south-north and west-east directions. The MYNN planetary boundary layer scheme (Nakanishi and Niino, 2006), CLM land surface scheme (Oleson et al., 2010), Morrison 2-moment microphysics scheme (Morrison et al., 2009), Kain-Fritsch cumulus scheme (Kain, 2004), and Rapid Radiative Transfer Model (RRTMG) longwave and shortwave radiation schemes (Iacono et al., 2000) are used in this study. The chemical initial and boundary conditions are provided by a quasi-global WRF-Chem simulation for the same time period to include long-range transported chemical species (Zhao et al., 2013b; Hu et al., 2016). The quasi-global WRF-Chem simulation is performed at 1° × 1° horizontal resolution using a quasi-global channel configuration with 360 × 130 grid cells (180°W-180°E, 60°S-70°N). More details about the quasi-global WRF-Chem simulation can be found in Zhao et al. (2013b) and Hu et al. (2016).

2.1.3 Emissions

Anthropogenic emissions for outer and inner simulation domains are obtained from the Hemispheric Transport of Air Pollution version-2 (HTAPv2) at 0.1° × 0.1° horizontal resolution and a monthly temporal resolution for year 2010 (Janssens-Maenhout et al., 2015),

https://doi.org/10.5194/acp-2019-905
Preprint. Discussion started: 14 October 2019

except that emissions over East and South Asia within the domains are from the MIX Asian anthropogenic emission inventory at 0.1°×0.1° horizontal resolution for 2015 (Li et al., 2017). Biomass burning emissions are obtained from the Fire Inventory from NCAR (FINN) with hourly temporal resolution and 1 km horizontal resolution (Wiedinmyer et al., 2011), and are vertically distributed following the injection heights suggested by Dentener et al. (2006) from the Aerosol Comparison between Observations and Models (AeroCom) project. Sea-salt emission follows Zhao et al. (2013), which includes correction of particles with radius less than 0.2 μm (Gong, 2003) and dependence of sea-salt emission on sea surface temperature (Jaeglé et al., 2011). The vertical dust fluxes are calculated with the GOCART dust emission scheme (Ginoux et al., 2001), and the emitted dust particles are distributed into the MOSAIC aerosol size bins following a theoretical expression based on the physics of scale-invariant fragmentation of brittle materials derived by Kok (2011). More details about the dust emission scheme coupled with MOSAIC aerosol scheme in WRF-Chem can be found in Zhao et al. (2010, 2013b).

As shown in Figure 1, anthropogenic fossil fuel emissions of BC are high over Northeast India. The fossil fuel BC emissions over Nepal, the country nearby the southern Himalayas, are relatively low. Instead, biomass burning emissions of BC are extremely high in Nepal and Northwest India (South Himalayas). On average over the inner domain, the biomass burning emission of BC is much higher than anthropogenic fossil fuel emissions, particularly for the pollution episode (Fig. 4). The anthropogenic BC emission is set constant through April, while biomass burning emission shows a strong fire event in April 5-16. During the event, the biomass burning BC emission can be a factor of 2 of the anthropogenic fossil fuel BC emission.

2.2 Dataset

Three datasets are used to compare with the modeling results to indicate the pollutant episode and spatial distribution. One is from the MODIS instruments on Aqua and Terra satellites. The MODIS Aerosol Product monitors the ambient aerosol optical thickness over the oceans globally and over the continents. Daily Level 2 aerosol optical depth (AOD) at 550 nm products with the spatial resolution of 10 km×10 km (at nadir) from both Aqua and Terra are applied. When compared with the modeling results, the simulations are sampled at the satellite overpass time and location. The second one is from the Aerosol Robotic Network (AERONET) (Holben et al., 1998) that has ~100 identical globally distributed sun- and sky-scanning ground-based automated radiometers, which provide measurements of aerosol

https://doi.org/10.5194/acp-2019-905
Preprint. Discussion started: 14 October 2019

optical properties throughout the world (Dubovik and King, 2000; Dubovik et al., 2002). In this study, AERONET measured AOD at 675 nm and 440 nm from two sites over the TP (QOMS, 86.56°E, 28.21°N; NAM, 90.96°E, 30.77°N) are used to derive the AOD at 600 nm (using the Angström exponent) for comparison with modeling results. All of the retrievals of AOD are at quality level 2, and the uncertainty of AOD measurements is about 0.01 (Holben et al., 2001). In this study, the available data in April 2016 are used to evaluate the modeling results during the same period. The third one is the measurement of surface BC mass concentration collected at the comprehensive observation and research station (QOMS) of the Everest and the Environment of the Chinese Academy of Sciences located at the northern slope of Himalayas (28.21°N and 86.56°E), about 4276 meters above sea level (Chen et al., 2018).

3. Results

3.1 Spatial distribution of BC around the TP

Figure 5 shows the spatial distribution of column integrated BC mass over the area with the terrain height larger than 0.5 km within the inner domain from the simulations at 20 km and 4 km resolutions averaged for April 5-20, 2016. The difference between the simulations at two resolutions is also shown. The wind fields at 500 hPa are also shown. The southern Himalayas is an apparent boundary line for the distribution of BC. There is a sharp gradient across the Himalayas. The high BC mass loading exists near the southern Himalayas reaching over 20 mg/m^2, while the value reduces significantly to less than 0.5 mg/m^2 over the TP. The high BC mass loading near the southern Himalayas is primarily contributed by the biomass burning emission during the period (Fig. 4). The relatively large difference between the two simulations over the source region near the southern Himalayas is mainly due to the different spatial distributions of emissions at the different resolutions. Over the TP, the column BC mass loading from the simulation at 4 km is higher than that at 20 km resolution. Figure 6 displays the spatial distributions of AOD from the MODIS retrievals and the simulations at 4 km and 20 km resolutions averaged for April 5-20, 2016. In general, the simulations reproduce the overall spatial distribution of AOD, with the large value near the southern Himalayas, consistent with the BC mass loading. The difference between the simulations and retrievals may be partly related to the uncertainties in emissions particularly for biomass burning emission. Not only the strong emission near the southern Himalayas, the wind circulations around the TP also play an important role in accumulating BC near the slope of

Himalayas. Because of the block of Himalayas, the wind circulation at 500 hPa is divided into two branches as westerly and northwesterly. Both of them are relatively dry airflows with little effect on pollutant removal. The westerlies favor the accumulation of pollutants near the southern Himalayas and can carry the pollutants to the TP (Vernekar et al., 2003; Ramanathan et al., 2008; Cong et al., 2015a). The MODIS AOD retrievals over the TP are scarce. The AOD retrieved at two AERONET sites over the TP are compared with the simulations at 4 km and 20 km resolutions for April, 2016 (Figure 7). The AOD at the QOMS site near the northern Himalayas is higher than that at the NAM site inside of the TP. The simulations at both resolutions can capture this gradient. The simulation at 4 km resolution produces higher AOD than does the one at 20 km resolution at both sites. The modeling biases (normalized mean bias, NMB) reduce from -28% (20 km resolution) to 11% (4 km resolution) at the QOMS site and from -58% (20 km resolution) to -10% (4 km resolution) at the NAM site.

Figure 8 shows the spatial distribution of surface BC concentration and surface wind field within the inner domain from the simulations at 4 km and 20 km resolutions. The difference between the simulations at two resolutions is also shown. Over the TP, the surface BC concentration near the Himalayas from the simulation at 4 km resolution is higher than that at 20 km resolution, but the difference between the two simulations is relatively small compared to the column BC mass (Fig. 5). The difference also exhibits heterogeneous distribution with evidently higher BC concentration at 4 km resolution than at 20 km resolution near the valleys, which reflects the impact of topography on transport (see the discussion in Section 3.2). Compared with the winds at 500 hPa (Fig. 5), surface winds show stronger southerlies reflecting local circulations, and this enhancement of southerlies is larger at 4 km resolution than at 20 km resolution. There is one observational site (QOMS) near the Mt. Everest (black dot shown in Fig. 8) to collect the surface BC concentration. The observed surface BC concentration at this site is compared with the corresponding simulations for this period as shown in Figure 9. Without local emission source, the surface BC concentration at QOMS is primarily contributed by the transport. The temporal variation of observed surface BC concentration correlated highly with the biomass burning emissions as shown in Fig. 4, with the peak BC concentration on April 11 reaching ~3.5 ug/m^3. This further proves that the BC concentration over the TP can be largely influenced by the pollution episode near the southern Himalayas. The simulations at both resolutions can reproduce the episode in time and magnitude. It is interesting to note that the difference in surface BC concentrations at this site between the simulations at 4 km and 20 km resolutions is small. This may be due to that

https://doi.org/10.5194/acp-2019-905
Preprint. Discussion started: 14 October 2019

the site is besides Mt. Everest and does not well reflect the difference between the simulations at 4 km and 20 km resolutions, which is shown primarily associated with the valley transport (see the discussion in Section 3.2).

3.2 Transport flux into the TP

To further understand the difference in BC surface concentration and column mass loading over the TP between the two simulations at resolutions of 4 km and 20 km, Figure 10 shows the longitude-height cross section of BC transport flux along the cross line (shown as the black dash line in Fig. 3) from the two simulations at local time (LT) 03:00 and 15:00 averaged for April 5-20 to represent nighttime and daytime transport, respectively. The PBL height along the cross line is also shown as the black line. The transport flux is calculated by projecting the wind fields perpendicularly to the cross line and then multiplying the BC mass concentration along the cross line. Positive value denotes the northward transport across the Himalayas, and negative value denotes the southward transport. It is evident that BC is imported into the TP during the day and night in the west to ~85°E, although the transport flux is much larger during the daytime than nighttime. In the east to ~85°E, BC is imported into the TP during the day but exported slightly from the TP during the night. The difference of transport flux between the west and east to ~85°E is primarily due to the influence of large-scale westerlies that is relatively weak in the east to ~85°E compared with the west (Fig. 5 and 8). If removing the background westerlies, i.e., transport flux anomalies by removing the mean flux averaged during the period, the transport flux dominated by the local circulation reverses between the day and night (Fig. S2 in the supporting material). This suggests that the large-scale westerlies are the dominant mechanism transporting BC across the Himalayas into the TP. The local circulation strengthens the prevailing import transport during the daytime and weakens the import during the night, particularly in the west to ~85°E. In addition, deeper PBL during the daytime allows BC over the source region mixed to higher altitude, which also leads to stronger import transport during the day than the night.

In general, the characteristics of transport flux across the Himalayas discussed above are consistent between the simulations at 4 km and 20 km resolutions. However, the difference between the two resolutions is also evident. First of all, the mountain ridges are much higher and valleys are much deeper at 4 km than at 20 km resolution. Overall, the topography is more smoothing at 20 km than at 4 km resolution. To demonstrate the transport pathway through valleys and across mountain ridges, the valley cross-section and the mountain cross-section shown as the two black lines in Fig. 3 are selected to show the transport

https://doi.org/10.5194/acp-2019-905
Preprint. Discussion started: 14 October 2019

mechanisms in Figure 11 and 12, respectively, from the simulations at 20 km and 4 km resolutions at LT 03:00 and 15:00 averaged for April 5-20, 2016. Near the southern part of both valley and mountain, the elevated concentrations of BC mass accumulate and can mix up reaching as high as 5 km. The spatial distributions of BC mass concentration between day and night are similar. Through the valley, the PBL is deeper during the daytime than nighttime. At both resolutions, uphill BC transport is evident in the day and night. The transport is primarily within the PBL during the daytime and is much stronger than that during the night. The transport flux anomalies by removing the mean flux averaged during the period show that the local circulation strengthens the uphill transport during the daytime but weakens the uphill transport during the night (Fig. S3 in the supporting material). The transport flux is much stronger at 4 km than at 20 km resolution for both daytime and nighttime. Although mountain ridges can hinder the crossing-Himalayas transport, Figure 12 shows evident transport fluxes from the southern foothill of Himalayas to the TP at both resolutions. The simulation at 20 km resolution produces similar results as that along the valley due to its smoothing topography. The simulation at 4 km resolution with the high mountain ridge can still produce efficient transport across the mountain ridge, although the flux is weaker than that through the valley. Similar as the transport through the valley, the local circulation strengthens (weakens) the uphill transport during the daytime (night) (Fig. S4 in the supporting material). The results above suggest that the BC accumulated near the southern Himalayas can be transported across the Himalayas no matter of through valleys or across mountain ridges, which is consistent with the observation-based estimate by Gong et al. (2019) that also found pollutants can overcome the blocking effect of mountain ridges of Himalayas as a transport pathway.

The vertically integrated BC mass fluxes distributed along the longitudinal cross section in Fig. 10 from the simulations at 20 km and 4 km resolutions are shown in Figure 13. The terrain heights along the cross section are also shown as black lines. Again, it shows that the topography at 4 km resolution is more complex than that at 20 km resolution with more mountain ridges and valleys. The positive import BC fluxes occur not only through the valleys but also across the mountain ridges at both resolutions. At 4 km resolution, although higher mountain ridges can reduce the transport flux to some extent compared to the relatively smoothing terrain at 20 km resolution, they cannot block the transport. On the other hand, the deeper valleys at 4 km resolution significantly enhance the transport compared to the 20 km resolution. All the enhancement of transport flux at 4 km resolution corresponds well to the deeper valleys such as the Karnali River Valley around 82°E and the Kali Gandaki

Atmospheric Chemistry and Physics Discussions

Valley around 84°E. This turns out that the overall transport at 4 km resolution is much stronger than that at 20 km resolution. Figure 14 shows the accumulated integrated total transport flux of BC across the Himalayas estimated from the simulations at 20 km and 4 km resolutions for April 1-20, 2016. The accumulated import flux of BC increases during the period at both resolutions, and the difference between the two resolutions gradually increases with the time. At the end of period, the simulation at 4 km resolution estimates a total import flux of BC of ~1.5×10^4 Ton that is ~50% higher than ~1.0×10^4 Ton estimated based on the simulation at 20 km resolution.

To confirm that the different modeling results between the two resolutions is due to their different complexity of topography of Himalayas, a sensitivity experiment is conducted in the same way as the control experiment except that the inner domain at 4 km resolution applies the topography distribution exactly following that at 20 km resolution. It is interesting that the sensitivity experiment simulates very similar transport flux of BC along the longitude cross section (Fig. 13 and 14). This indicates that the difference between the simulations at the two resolutions is primarily determined by their difference of topography, which highlights the significant impact of the complexity of topography on BC transport across the Himalayas. The simulation at 4 km resolution resolves more valleys and thus produces much stronger transport fluxes, which indicates that although the transport of South Asian BC across the Himalayas can overcome the mountain ridges, the valley transport is much more efficient and this enhancement cannot be ignored.

3.3 Radiative forcing of BC over the TP

The BC transported over the TP could significantly influence the regional climate and water resources over Asia through heating the atmosphere and accelerating the melting of snow and glacier (e.g., Qian et al., 2011, 2015; Lau et al., 2016, 2017). Therefore, the impact of the complex topography on estimating the BC radiative heating profile in the atmosphere and radiative forcing in surface snow deserves investigation. Figure 15 shows the vertical profile of BC induced radiative heating rate in the atmosphere averaged over the TP (with elevation > 4 km) within the inner domain shown in Fig. 1 for April 5-20, 2016 from the simulations at 20 km and 4 km resolutions. The result from the sensitivity experiment at 4 km but with the smoothing 20km-topography is also shown. The simulations at both resolutions generate higher BC heating rate near the surface and the rate gradually decreases with altitude, which is consistent with the vertical profiles of BC mass concentration averaged

https://doi.org/10.5194/acp-2019-905
Preprint. Discussion started: 14 October 2019

over the TP (Fig. S5 in the supporting material). The BC heating rate over the TP from the simulation at 4 km resolution is ~0.17 K/day near the surface and reduces to ~0.08 K/day at 8 km, which are ~20% and ~50%, respectively, higher than that from the simulation at 20 km resolution at the corresponding altitudes. The higher BC heating rate over the TP estimated by the simulation at 4 km resolution is consistent with its higher BC column mass (Fig. 5) and concentration profile (Fig. S5). The sensitivity experiment at 4 km resolution with the smoothing 20km-topography simulates more similar BC heating profile as that from the experiment at 20 km resolution, which is consistent with the vertical profiles of BC mass concentration (Fig. S5). However, it is noteworthy that with the same topography, the sensitivity experiment at 4 km resolution produces significantly lower BC mass concentration and heating rate near the surface than the one at 20 km resolution. The process analysis indicates that this is mainly due to that the sensitivity experiment simulates smaller net transported BC concentration near the surface of TP compared to the experiment at 20 km resolution (not shown).

The BC radiative forcing in surface snow is controlled by both the distributions of BC mass concentration and snow coverage (e.g., Zhao et al., 2014). Figure 16 shows the spatial distributions of snow water equivalent (SWE) averaged for April 5-20, 2016 from the simulations at 20 km and 4 km resolutions. The sensitivity experiment at 4 km resolution but with the smoothing 20km-topography is also shown. It shows that the simulation at 4 km resolution generates more areas with higher SWE compared to that at 20 km resolution. In particular, the SWE is higher over the mountain ridges along the Himalayas and over the TP at 4 km than at 20 km resolution. The sensitivity experiment at 4 km resolution but with the smoothing 20km-topography still produces larger SWE along the Himalayas but similar SWE over the TP compared to the simulation at 20 km resolution. This is mainly induced by the difference in precipitation between the two resolutions (Fig. S6 in the supporting material). Along the Himalayas, the precipitation from the simulation at 4 km resolution is larger than that at 20 km resolution regardless of the complexity of topography. However, over the TP, larger precipitation is produced with more complex topography at 4 km resolution than that at 20 km resolution (Fig. S6).

Figure 17 shows the spatial distributions of BC radiative forcing in the surface snow over the TP averaged for April 5-20, 2016 from the simulations at 20 km and 4 km resolutions. The sensitivity experiment at 4 km resolution but with the smoothing 20km-topography is also shown. The BC radiative forcing in surface snow is largely coincident with the spatial distributions of SWE as shown in Fig. 16, mainly due to the

https://doi.org/10.5194/acp-2019-905
Preprint. Discussion started: 14 October 2019

heterogeneous distributions of snow cover over the TP. The BC radiative forcing in surface snow over the TP from the simulation at 4 km resolution reaches 6 W/m^2 where the snow exists, much larger than that at 20 km resolution. Along the Himalayas, the simulation at 4 km produces BC snow forcing over mountains almost along the entire Himalayas, while the one at 20 km resolution only has the considerable BC snow forcing over the western Himalayas, which follows the distributions of snow coverage along the Himalayas (Fig. 16). Over the western Himalayas, the simulation at 20 km resolution generates higher BC forcing in snow to some extent. With the smoothing 20km-topography at the 4 km resolution, the simulated BC forcing in snow covers more areas along the Himalayas than that from the 20 km resolution and is similar as that at the simulation at 4 km resolution. However, with the smoothing 20km-topography, the BC forcing in snow from the simulation at 4 km resolution is higher over the western Himalayas. Overall, the complex topography at 4 km leads to higher BC forcing in snow over the TP and the eastern Himalayas and reduces the BC forcing in snow over the western Himalayas, and therefore results in a different distribution of BC forcing in snow over the TP and Himalayas, compared to that at 20 km resolution.

4. Summary and discussion

In this study, the model experiments at different resolutions are conducted to illustrate the impacts of complexity of topography of Himalayas on BC transport from South Asia to the TP. The observed pollution episode at the QOMS station besides the Mt. Everest during the pre-monsoon season is simulated. The observed surface BC concentrations show a peak of ~3.5 ug/m^3 much larger than the background value of < 0.5 ug/m^3 over the TP. The observed temporal variation of surface BC concentrations correlates highly with that of biomass burning emissions near the southern Himalayas, indicating the significant impacts of biomass burning on the pollutants over the TP. The simulations can reproduce the episode in time and magnitude, and are used to investigate the BC transport mechanisms and the impacts of topography.

The high BC mass loading during the simulation period accumulates near the southern Himalayas driven by the large-scale circulation, which is also observed by satellites. The modeling results demonstrate that the westerlies favor the accumulation of pollutants near the southern Himalayas and can carry the pollutants to the TP during the day and night, which is consistent with previous modeling studies (e.g., Kopacz et al., 2011). The transport is stronger across the West Himalayas than that across the East. The local circulation strengthens the prevailing import transport during the daytime and weakens the import during the night. In addition, deeper PBL during the daytime allows BC over the source region mixed to higher altitude, which also leads to stronger import transport during the day than the night. It is also noteworthy that the BC accumulated near the southern Himalayas can be transported across the Himalayas no matter of through valleys or across mountain ridges, which is consistent with the observation-based estimate by Gong et al. (2019) that also found pollutants can overcome the blocking effect of the mountain ridges of Himalayas as the efficient transport pathway. However, the transport through the valleys is found much stronger and more efficient than across the mountain ridges and the enhancement effect cannot be ignored.

The mountain ridges are much higher and valleys are much deeper at 4 km resolution than at 20 km resolution. The transport strength through the valleys and across the mountains are similar from the simulation at 20 km resolution due to its smoothing topography. At 4 km resolution, the deeper valleys result in much stronger transport flux than that at 20 km resolution, which highlights the significant impact of the complexity of topography on BC transport across the Himalayas. The complex topography resolved by the 4 km resolution leads to 50% higher overall transport fluxes of BC across the Himalayas compared to that from the simulation at 20 km resolution during the simulation period. This turns out that the simulation at 4 km resolution produces 20-50% higher BC radiative heating rate in the atmosphere averaged over the TP than does the simulation at 20 km resolution. For the BC radiative forcing in surface snow, the simulation at 4 km resolution produces stronger forcing over the TP than that at 20 km resolution. The complex topography makes the distribution of BC forcing in surface snow quite different between the simulations at the two resolutions, partly due to their different distributions of surface snow. The simulated BC radiative forcing in snow are distributed more heterogeneously than those in previous studies using global models at relatively coarse resolutions (e.g., Qian et al., 2011). He et al. (2014) used a global chemical transport model to simulate the BC forcing in snow at the horizontal resolution of ~0.2° and obtained the similar distribution as this study with the high values over the western Himalayas. However, their simulated values near the Himalayas are higher than the simulated results at 20 km resolution of this study and are close to the results at 4 km resolution, which may be due to their estimation are averaged for November-April.

This study highlights the importance of resolving complex topography of the Himalayas in modeling the aerosol radiative impact over the TP. Climate models at coarser horizontal resolutions than 20 km may underestimate the aerosol transport from South Asia to the TP

https://doi.org/10.5194/acp-2019-905
Preprint. Discussion started: 14 October 2019

Atmospheric Chemistry and Physics Discussions

during the pre-monsoon season and represent inappropriately the aerosol radiative forcing in the atmosphere and surface snow over the TP. In addition, aerosol impact on cloud and precipitation, particularly during the monsoon season, and thus on the latent heat in the atmosphere and the associated responses may also depend on the complex topography. Previous studies based on observations found that the rain frequency and intensity reached the highest and the cloud thickness reached the deepest at the foothill of Himalayas and decreased as the elevation increased up to the TP (e.g., Chen et al., 2017; Fu et al., 2018; Zhang et al., 2018), which was explained by Fu et al. (2018) due to the blocking of the air flow by the steep slope of southern Himalayas. However, the large amount of transported aerosol along the slope from the foothill up to the TP may also play a role. These potential impacts of aerosols on regional hydro-climate around the TP and over Asia using high-resolution model that can resolve the complex topography of Himalayas and TP deserve further investigation.

Data availability

The released version of WRF-Chem can be downloaded from http://www2.mmm.ucar.edu/wrf/users/download/get_source.html. The updated USTC version of WRF-Chem can be downloaded from http://aemol.ustc.edu.cn/product/list/ or contact chunzhao@ustc.edu.cn. Also, the code modifications will be incorporated the release version of WRF-Chem in future.

Author contributions

Meixin Zhang and Chun Zhao designed the experiments, conducted and analyzed the simulations. All authors contributed to the discussion and final version of the paper.

Acknowledgements

This research was supported by the National Key Research and Development Program of China (2016YFA0602001), the National Natural Science Foundation of China NSFC (Grant No. 91837310), the second Tibetan Plateau Scientific Expedition and Research Program (STEP) (2019QZKK0605), and the Fundamental Research Funds for the Central Universities. The study used computing resources from the High-Performance Computing Center of University of Science and Technology of China (USTC) and the TH-2 of National Supercomputer Center in Guangzhou (NSCC-GZ).

https://doi.org/10.5194/acp-2019-905
Preprint. Discussion started: 14 October 2019

Reference

Barnard, J. C., Fast, J. D., Paredes-Miranda, G., Arnott, W. P., and Laskin, A.: Technical Note: Evaluation of the WRF-Chem "Aerosol Chemical to Aerosol Optical Properties" Module using data from the MILAGRO campaign, Atmos. Chem. Phys., 10, 7325–7340, doi: 10.5194/acp-10-7325-2010, 2010.

Barnett, T. P., Adam, J. C., and Lettenmaier, D. P.: Potential impacts of a warming climate on water availability in snow-dominated regions, Nature, 438, 303–309, doi: 10.1038/nature04141, 2005.

Binkowski, F. S. and Shankar, U.: The Regional Particulate Matter Model: 1. Model description and preliminary results, J. Geophys. Res., 100, 26191, doi: 10.1029/95JD02093, 1995.

Boos, W. R. and Kuang, Z.: Sensitivity of the South Asian monsoon to elevated and non-elevated heating, Scientific reports, 3, 1192, doi: 10.1038/srep01192, 2013.

Brun, J., Shrestha, P., and Barros, A. P.: Mapping aerosol intrusion in Himalayan valleys using the Moderate Resolution Imaging Spectroradiometer (MODIS) and Cloud–Aerosol Lidar and Infrared Pathfinder Satellite Observation (CALIPSO), Atmospheric Environment, 45, 6382–6392, doi: 10.1016/j.atmosenv.2011.08.026, 2011.

Cao, J., Tie, X., Xu, B., Zhao, Z., Zhu, C., Li, G., and Liu, S.: Measuring and modeling black carbon (BC) contamination in the SE Tibetan Plateau, Journal of Atmospheric Chemistry, 67, 45-60, doi: 10.1007/s10874-011-9202-5, 2010.

Chapman, E. G., Gustafson, W. I., Easter, R. C., Barnard, J. C., Ghan, S. J., Pekour, M. S., and Fast, J. D.: Coupling aerosol-cloud-radiative processes in the WRF-Chem model: Investigating the radiative impact of elevated point sources, Atmos. Chem. Phys., 9, 945–964, doi: 10.5194/acp-9-945-2009, 2009.

Chen, J. and Bordoni, S.: Orographic Effects of the Tibetan Plateau on the East Asian Summer Monsoon: An Energetic Perspective, J. Climate, 27, 3052–3072, doi: 10.1175/JCLI-D-13-00479.1, 2014.

Chen, P., Li, C., Kang, S., Rupakheti, M., Panday, A. K., Yan, F., Li, Q., Zhang, Q., Guo, J., Ji, Z., Rupakheti, D., and Luo, W.: Characteristics of Particulate-Phase Polycyclic Aromatic Hydrocarbons (PAHs) in the Atmosphere over the Central Himalayas, Aerosol Air Qual. Res., 17, 2942–2954, doi: 10.4209/aaqr.2016.09.0385, 2017.

Chen, X., Kang, S., Cong, Z., Yang, J., and Ma, Y.: Concentration, temporal variation, and sources of black carbon in the Mt. Everest region retrieved by real-time observation and simulation, Atmos. Chem. Phys., 18, 12859–12875, doi: 10.5194/acp-18-12859-2018, 2018.

Chen, Y.L., Fu, Y.F., Xian, T., Pan, X., 2017. Characteristics of cloud cluster over the steep southern slopes of the Himalayas observed by CloudSat. Int. J. Climatol. 37, 4043–4052.

Cong, Z., Kang, S., and Qin, D.: Seasonal features of aerosol particles recorded in snow from Mt. Qomolangma (Everest) and their environmental implications, Journal of environmental sciences (China), 21, 914–919, doi: 10.1016/S1001-0742(08)62361-X, 2009.

Cong, Z., Kang, S., Gao, S., Zhang, Y., Li, Q., and Kawamura, K.: Historical Trends of Atmospheric Black Carbon on Tibetan Plateau As Reconstructed from a 150-Year Lake Sediment Record, Environ. Sci. Technol., 47, 2579–2586,doi: 10.1021/es3048202, 2013.

Cong, Z., Kang, S., Kawamura, K., Liu, B., Wan, X., Wang, Z., Gao, S., and Fu, P.: Carbonaceous aerosols on the south edge of the Tibetan Plateau: concentrations, seasonality and sources, Atmos. Chem. Phys., 15, 1573–1584, doi: 10.5194/acp-15-1573-2015, 2015(a).

Cong, Z., Kawamura, K., Kang, S., and Fu, P.: Penetration of biomass-burning emissions from South Asia through the Himalayas: new insights from atmospheric organic acids, Scientific reports, 5, 9580, doi: 10.1038/srep09580, 2015(b).

Dentener, F., Kinne, S., Bond, T., Boucher, O., Cofala, J., Generoso, S., Ginoux, P., Gong, S., Hoelzemann, J. J., Ito, A., Marelli, L., Penner, J. E., Putaud, J.-P., Textor, C., Schulz, M., van der Werf, G. R., and Wilson, J.: Emissions of primary aerosol and precursor gases in the years 2000 and 1750, prescribed data-sets for AeroCom, Atmos. Chem. Phys. Discuss., 6, 2703–2763, doi: 10.5194/acpd-6-2703-2006, 2006.

Dhungel, S., Kathayat, B., Mahata, K., and Panday, A.: Transport of regional pollutants through a remote trans-Himalayan valley in Nepal, Atmos. Chem. Phys. Discuss., 1–23, doi: 10.5194/acp-2016-824, 2016.

Ding, Y., Sun, Y., Wang, Z., Zhu, Y., and Song, Y.: Inter-decadal variation of the summer precipitation in China and its association with decreasing Asian summer monsoon Part II: Possible causes, Int. J. Climatol., 29, 1926–1944, doi: 10.1002/joc.1759, 2009.

Duan, A. M. and Wu, G. X.: Role of the Tibetan Plateau thermal forcing in the summer climate patterns over subtropical Asia, Climate Dynamics, 24, 793–807, doi: 10.1007/s00382-004-0488-8, 2005.

Dumka, U. C., Moorthy, K. K., Kumar, R., Hegde, P., Sagar, R., Pant, P., Singh, N., and Babu, S. S.: Characteristics of aerosol black carbon mass concentration over a high altitude

https://doi.org/10.5194/acp-2019-905
Preprint. Discussion started: 14 October 2019

Atmospheric Chemistry and Physics Discussions

location in the Central Himalayas from multi-year measurements, Atmospheric Research, 96, 510–521, doi: 10.1016/j.atmosres.2009.12.010, 2010.

Dubovik, O., and King, M. D.: A flexible inversion algorithm for retrieval of aerosol optical properties from sun and sky radiance measurements, J. Geophys. Res., 105, 20673–20696, 2000.

Dubovik, O., Holben, B., Eck, T. F., Smirnov, A., Kaufman, Y.J., King, M.D., Tanre, D., and Slutsker, I.: Variability of absorption and optical properties of key aerosol types observed in worldwide locations, J. Atmos. Sci., 59, 590-608, 2002.

Easter, R. C., Ghan, S. J., Zhang, Y., Saylor, R. D., Chapman, E. G., Laulainen, N. S., Abdul-Razzak, H., Leung, L. R., Bian, X., and Zaveri, R. A.: MIRAGE: Model Description and Evaluation of Aerosols and Trace Gases, J. Geophys. Res., 109, D20210, doi:10.1029/2004JD004571, 2004.

Engling, G. and Gelencser, A.: Atmospheric Brown Clouds: From Local Air Pollution to Climate Change, Elements, 6, 223–228, doi: 10.2113/gselements.6.4.223, 2010.

Fast, J. D., Gustafson Jr, W. I., Easter, R. C., Zaveri, R. A., Barnard, J. C., Chapman, E. G., Grell, G. A., and Peckham, S. E.: Evolution of ozone, particulates, and aerosol direct radiative forcing in the vicinity of Houston using a fully coupled meteorology-chemistry-aerosol model, J. Geophys. Res., 111, D21305, doi: 10.1029/2005JD006721, 2006.

Flanner, M. G. and Zender, C. S.: Snowpack radiative heating: Influence on Tibetan Plateau climate, Geophys. Res. Lett., 32, L06501, doi: 10.1029/2004GL022076, 2005.

Fu, Y., Pan, X., Xian, T., Liu, G., Zhong, L., Liu, Q., Li, R., Wang, Y., 2018. Precipitation characteristics over the steep slope of the Himalayas observed by TRMM PR and VIRS. Clim. Dyn. http://dx.doi.org/10.1007/s00382-017-3992-3.

Gautam, R., Hsu, N. C., Tsay, S. C., Lau, K. M., Holben, B., Bell, S., Smirnov, A., Li, C., Hansell, R., Ji, Q., Payra, S., Aryal, D., Kayastha, R., and Kim, K. M.: Accumulation of aerosols over the Indo-Gangetic plains and southern slopes of the Himalayas: distribution, properties and radiative effects during the 2009 pre-monsoon Season, Atmos. Chem. Phys. Discuss., 11, 15697–15743, doi: 10.5194/acpd-11-15697-2011, 2011.

Ginoux, P., Chin, M., Tegen, I., Prospero, J. M., Holben, B., Dubovik, O., and Lin, S.-J.: Sources and distributions of dust aerosols simulated with the GOCART model, J. Geophys. Res., 106, 20255–20273, doi: 10.1029/2000JD000053, 2001.

Gong, P., Wang, X.-p., Pokhrel, B., Wang, H., Liu, X., Liu, X., and Wania, F.: Trans-Himalayan transport of organochlorine compounds: three-year observations and model-based flux estimation, Environ. Sci. Technol., 53, 6773−6783, doi: 10.1021/acs.est.9b01223, 2019.

Gong, S. L.: A parameterization of sea-salt aerosol source function for sub- and super-micron particles, Global Biogeochem. Cycles, 17, n/a-n/a, doi: 10.1029/2003GB002079, 2003.

Grell, G. A., Peckham, S. E., Schmitz, R., McKeen, S. A., Frost, G., Skamarock, W. C., and Eder, B.: Fully coupled "online" chemistry within the WRF model, Atmospheric Environment, 39, 6957–6975, doi: 10.1016/j.atmosenv.2005.04.027, 2005.

Gustafson, W. I., E. G. Chapman, S. J. Ghan, R. C. Easter, and J. D. Fast: Impact on modeled cloud characteristics due to simplified treatment of uniform cloud condensation nuclei during NEAQS 2004, Geophys. Res. Lett., 34, L19809, doi:10.1029/2007GL030021, 2007.

Hansen, J. and Nazarenko, L.: Soot climate forcing via snow and ice albedos, Proceedings of the National Academy of Sciences, 101, 423–428, doi: 10.1073/pnas.2237157100, 2004.

He, C., Li, Q., Liou, K.-N., Takano, Y., Gu, Y., Qi, L., Mao, Y., and Leung, L. R.: Black carbon radiative forcing over the Tibetan Plateau, Geophys. Res. Lett., 41, 7806–7813, doi: 10.1002/2014GL062191, 2014.

He, C., Wang, Z., Zhou, T., and Li, T.: Enhanced Latent Heating over the Tibetan Plateau as a Key to the Enhanced East Asian Summer Monsoon Circulation under a Warming Climate, J. Climate, 32, 3373–3388, doi: 10.1175/JCLI-D-18-0427.1, 2019.

Hess, M., Koepke, P., and Schult, I.: Optical Properties of Aerosols and Clouds: The Software Package OPAC, Bull. Amer. Meteor. Soc., 79, 831–844, doi: 10.1175/1520-0477(1998)079<0831:OPOAAC>2.0.CO;2, 1998.

Hindman, E. E. and Upadhyay, B. P.: Air pollution transport in the Himalayas of Nepal and Tibet during the 1995–1996 dry season, Atmospheric Environment, 36, 727–739, doi: 10.1016/S1352-2310(01)00495-2, 2002.

Holben, B. N., Eck, T. F., Slutsker, I., Tanr' e, D., Buis, J. P., Stezer, A., Vermote, E., Reagan, Y., Kaufman, U. J., Nakajima, T., Lavenu, F., Jankowiak, I., and Smirnov, A.: AERONET-A federated instrument network and data archive for aerosol characterization, Rem. Sens. Environ., 66, 1–16, 1998.

Holben, B. N., Tanre, D., Smirnov, A., ECK T. F., Slutsker, I., Abuhassan, N., Newcomb, W., Schafer, J., Chatenet, B., Lavenu, F., Kaufman, Y., Vande Castle, J., Setzer, A., Markham, B., Clark, D., Frouin, R., Halthore, R., Karneli, A., O'Neill, N., Pietras, C., Pinker, R.,

https://doi.org/10.5194/acp-2019-905
Preprint. Discussion started: 14 October 2019

Voss, K., and Zibordi, G.: An emerging ground-based aerosol climatology: Aerosol optical depth from AERONET, J. Geophys. Res., 106, 12067-12097, 2001.

Hu, Z., Zhao, C., Huang, J., Leung, L. R., Qian, Y., Yu, H., Huang, L., and Kalashnikova, O. V.: Trans-pacific transport and evolution of aerosols: Evaluation of quasi global WRF-Chem simulation with multiple observations, Geosci. Model Dev. Discuss., 1–65, doi: 10.5194/gmd-2015-248, 2016.

Hu, Z., Huang, J., Zhao, C., Bi, J., Jin, Q., Qian, Y., Leung, L. R., Feng, T., Chen, S., and Ma, J.: Modeling the contributions of Northern Hemisphere dust sources to dust outflow from East Asia, Atmospheric Environment, 202, 234–243, doi: 10.1016/j.atmosenv.2019.01.022, 2019.

Iacono, M. J., Mlawer, E. J., Clough, S. A., and Morcrette, J.-J.: Impact of an improved longwave radiation model, RRTM, on the energy budget and thermodynamic properties of the NCAR community climate model, CCM3, J. Geophys. Res., 105, 14873–14890, 2000.

Immerzeel WW, van Beek LPH and Bierkens MFP. Climate change will affect the Asian water towers. Science 2010; 328: 1382–5.

Jaeglé, L., Quinn, P. K., Bates, T. S., Alexander, B., and Lin, J.-T.: Global distribution of sea salt aerosols: new constraints from in situ and remote sensing observations, Atmos. Chem. Phys., 11, 3137–3157, doi: 10.5194/acp-11-3137-2011, 2011.

Janssens-Maenhout, G., Crippa, M., Guizzardi, D., Dentener, F., Muntean, M., Pouliot, G., Keating, T., Zhang, Q., Kurokawa, J., Wankmüller, R., van der Denier Gon, H., Kuenen, J. J. P., Klimont, Z., Frost, G., Darras, S., Koffi, B., and Li, M.: HTAP_v2.2: a mosaic of regional and global emission grid maps for 2008 and 2010 to study hemispheric transport of air pollution, Atmos. Chem. Phys., 15, 11411–11432, doi: 10.5194/acp-15-11411-2015, 2015.

Ji, Z., Kang, S., Cong, Z., Zhang, Q., and Yao, T.: Simulation of carbonaceous aerosols over the Third Pole and adjacent regions: distribution, transportation, deposition, and climatic effects, Clim Dyn, 45, 2831–2846, doi: 10.1007/s00382-015-2509-1, 2015.

Ji, Z.-M.: Modeling black carbon and its potential radiative effects over the Tibetan Plateau, Advances in Climate Change Research, 7, 139–144, doi: 10.1016/j.accre.2016.10.002, 2016.

Kain, J. S.: The Kain–Fritsch convective parameterization: An update, J. Appl. Meteorol., 43, 170–181, 2004.

Kang, S., Xu, Y., You, Q., Flügel, W.-A., Pepin, N., and Yao, T.: Review of climate and cryospheric change in the Tibetan Plateau, Environ. Res. Lett., 5, 15101, doi: 10.1088/1748-9326/5/1/015101, 2010.

Kang, S.: Atmospheric Aerosol Elements over the Inland Tibetan Plateau: Concentration, Seasonality, and Transport, Aerosol Air Qual. Res., doi: 10.4209/aaqr.2015.02.0307, 2015.

Kang, S., Q. Zhang, Y. Qian, Z. Ji, C. Li, Z. Cong, Y. Zhang, J. Guo, W. Du, J. Huang, Q. You, A. K. Panday, M. Rupakheti, D. Chen, O. Gustafsson, M. H. Thiemens, and D. Qin: Linking atmospheric pollution to cryospheric change in the Third Pole region: current progress and future prospects, National Science Review, 6, 796–809, doi: 10.1093/nsr/nwz031, 2019.

Kok, J. F.: A scaling theory for the size distribution of emitted dust aerosols suggests climate models underestimate the size of the global dust cycle, Proceedings of the National Academy of Sciences of the United States of America, 108, 1016–1021, doi: 10.1073/pnas.1014798108, 2011.

Kopacz, M., Mauzerall, D. L., Wang, J., Leibensperger, E. M., Henze, D. K., and Singh, K.: Origin and radiative forcing of black carbon transported to the Himalayas and Tibetan Plateau, Atmos. Chem. Phys., 11, 2837–2852, doi: 10.5194/acp-11-2837-2011, 2011.

Kuhlmann, J. and Quaas, J.: How can aerosols affect the Asian summer monsoon? Assessment during three consecutive pre-monsoon seasons from CALIPSO satellite data, Atmos. Chem. Phys. Discuss., 10, 4887–4926, doi: 10.5194/acpd-10-4887-2010, 2010.

Lau, K. M., Kim, M. K., and Kim, K. M.: Asian summer monsoon anomalies induced by aerosol direct forcing: the role of the Tibetan Plateau, Clim Dyn, 26, 855–864, doi: 10.1007/s00382-006-0114-z, 2006(a).

Lau, K.-M. and Kim, K.-M.: Observational relationships between aerosol and Asian monsoon rainfall, and circulation, Geophys. Res. Lett., 33, D22101, doi: 10.1029/2006GL027546, 2006(b).

Lau, W. K. M., Kim, M.-K., Kim, K.-M., and Lee, W.-S.: Enhanced surface warming and accelerated snow melt in the Himalayas and Tibetan Plateau induced by absorbing aerosols, Environ. Res. Lett., 5, 25204, doi: 10.1088/1748-9326/5/2/025204, 2010.

Lau, W. K. M. and Kim, K.-M.: Impacts of aerosols on the Asian Monsoon—An interim assessment, Climate Change: Multidecadal and Beyond, 361–376, doi: 10.1142/9789814579933_0023, 2016.

Lau, W. K. M., Kim, K.-M., Shi, J.-J., Matsui, T., Chin, M., Tan, Q., Peters-Lidard, C., and Tao, W. K.: Impacts of aerosol–monsoon interaction on rainfall and circulation over

https://doi.org/10.5194/acp-2019-905
Preprint. Discussion started: 14 October 2019

Atmospheric Chemistry and Physics Discussions
Open Access

Northern India and the Himalaya Foothills, Clim Dyn, 49, 1945–1960, doi: 10.1007/s00382-016-3430-y, 2017.

Lau, W.K.M.; Kim, K.-M. Impact of Snow Darkening by Deposition of Light-Absorbing Aerosols on Snow Cover in the Himalayas–Tibetan Plateau and Influence on the Asian Summer Monsoon: A Possible Mechanism for the Blanford Hypothesis. Atmosphere, 9, 438, doi: 10.3390/atmos9110438, 2018.

Lee, W.-S., Bhawar, R. L., Kim, M.-K., and Sang, J.: Study of aerosol effect on accelerated snow melting over the Tibetan Plateau during boreal spring, Atmospheric Environment, 75, 113–122, doi: 10.1016/j.atmosenv.2013.04.004, 2013.

Li, C., Bosch, C., Kang, S., Andersson, A., Chen, P., Zhang, Q., Cong, Z., Chen, B., Qin, D., and Gustafsson, Ö.: Sources of black carbon to the Himalayan–Tibetan Plateau glaciers, Nat Commun, 7, 4825, doi: 10.1038/ncomms12574, 2016.

Li, M., Zhang, Q., Kurokawa, J.-i., Woo, J.-H., He, K., Lu, Z., Ohara, T., Song, Y., Streets, D. G., Carmichael, G. R., Cheng, Y., Hong, C., Huo, H., Jiang, X., Kang, S., Liu, F., Su, H., and Zheng, B.: MIX: a mosaic Asian anthropogenic emission inventory under the international collaboration framework of the MICS-Asia and HTAP, Atmos. Chem. Phys., 17, 935–963, doi: 10.5194/acp-17-935-2017, 2017.

Li, R., and Q.-L. Min, 2010: Impacts of mineral dust on the vertical structure of precipitation, J. Geophys. Res., 115, D09203, doi:10.1029/2009JD011925.

Li, R., X. Dong, J. Guo, Y. Fu, Y. Wang, Q. Min, 2017: The implications of dust ice nuclei effect on cloud top temperature in a complex mesoscale convective system, Scientific Reports，7：13826，doi:10.1038/s41598-017-12681-0

Li, R., W. Shao, J. Guo, Y. Fu, G. Liu, Y. Wang, W. Li, 2019: A Simplified Algorithm to Estimate Latent Heating Rate Using Vertical Rainfall Profiles over the Tibetan Plateau, J. Geophys. Res. Atmos.,124,DOI: https://doi.org/10.1029/2018JD029297

Liu, P., Tsimpidi, A. P., Hu, Y., Stone, B., Russell, A. G., and Nenes, A.: Differences between downscaling with spectral and grid nudging using WRF, Atmos. Chem. Phys., 12, 3601–3610, doi: 10.5194/acp-12-3601-2012, 2012.

Liu, Y., Sato, Y., Jia, R., Xie, Y., Huang, J., and Nakajima, T.: Modeling study on the transport of summer dust and anthropogenic aerosols over the Tibetan Plateau, Atmos. Chem. Phys. Discuss., 15, 15005–15037, doi: 10.5194/acpd-15-15005-2015, 2015.

https://doi.org/10.5194/acp-2019-905
Preprint. Discussion started: 14 October 2019

Lu, Z., Streets, D. G., Zhang, Q., and Wang, S.: A novel back-trajectory analysis of the origin of black carbon transported to the Himalayas and Tibetan Plateau during 1996-2010, Geophys. Res. Lett., 39, n/a-n/a, doi: 10.1029/2011GL049903, 2012.

Lüthi, Z. L., Škerlak, B., Kim, S.-W., Lauer, A., Mues, A., Rupakheti, M., and Kang, S.: Atmospheric brown clouds reach the Tibetan Plateau by crossing the Himalayas, Atmos. Chem. Phys., 15, 6007–6021, doi: 10.5194/acp-15-6007-2015, 2015.

Lutz, A. F., Immerzeel, W. W., Shrestha, A. B., and Bierkens, M. F. P.: Consistent increase in High Asia's runoff due to increasing glacier melt and precipitation, Nature Clim Change, 4, 587–592, doi: 10.1038/nclimate2237, 2014.

Marinoni, A., Cristofanelli, P., Laj, P., Duchi, R., Calzolari, F., Decesari, S., Sellegri, K., Vuillermoz, E., Verza, G. P., and Villani, P.: Aerosol mass and black carbon concentrations, a two year record at NCO-P (5079 m, Southern Himalayas), Atmos. Chem. Phys., 10, 8551–8562, doi: 10.5194/acp-10-8551-2010, 2010.

Menon, S., Koch, D., Beig, G., Sahu, S., Fasullo, J., and Orlikowski, D.: Black carbon aerosols and the third polar ice cap, Atmos. Chem. Phys., 10, 4559–4571, doi: 10.5194/acp-10-4559-2010, 2010.

Ming, J., Cachier, H., Xiao, C., Qin, D., Kang, S., Hou, S., and Xu, J.: Black carbon record based on a shallow Himalayan ice core and its climatic implications, Atmos. Chem. Phys., 8, 1343–1352, 2008.

Ming, J., Xiao, C., Cachier, H., Qin, D., Qin, X., Li, Z., and Pu, J.: Black Carbon (BC) in the snow of glaciers in west China and its potential effects on albedos, Atmospheric Research, 92, 114–123, doi: 10.1016/j.atmosres.2008.09.007, 2009.

Mlawer, E. J., Taubman, S. J., Brown, P. D., Iacono, M. J., and Clough, S. A.: Radiative transfer for inhomogeneous atmospheres: RRTM, a validated correlated-k model for the longwave, J. Geophys. Res., 102, 16663–16682, 1997.

Morrison, H., Thompson, G., and Tatarskii, V.: Impact of Cloud Microphysics on the Development of Trailing Stratiform Precipitation in a Simulated Squall Line: Comparison of One- and TwoMoment Schemes, Mon. Weather Rev., 137, 991–1007, 2009.

Nakanishi, M. and Niino, H.: An Improved Mellor–Yamada Level-3 Model: Its Numerical Stability and Application to a Regional Prediction of Advection Fog, Boundary-Layer Meteorol, 119, 397–407, doi:10.1007/s10546-005-9030-8, 2006.

Oleson, K. W., Lawrence, D. M., Bonan, G. B., Flanner, M. G., Kluzek, E., Lawrence, P. J., Levis, S., Swenson, S. C., Thornton, P. E., Dai, A., Decker, M., Dickinson, R., Feddema,

https://doi.org/10.5194/acp-2019-905
Preprint. Discussion started: 14 October 2019

J., Heald, C. L., Hoffman, F., Lamarque, J.-F., Mahowald, N., Niu, G.-Y., Qian, T., Randerson, J., Running, S., Sakaguchi, K., Slater, A., Sto ckli, R., Wang, A., Yang, Z.-L., Zeng, X., and Zeng, X.: Tech- nical Description of version 4.0 of the Community Land Model (CLM), Tech. Rep. NCAR/TN-478 + STR, National Center for Atmospheric Research, 2010.

Prasad, A. K. and Singh, R. P.: Comparison of MISR-MODIS aerosol optical depth over the Indo-Gangetic basin during the winter and summer seasons (2000–2005), Remote Sensing of Environment, 107, 109–119, doi: 10.1016/j.rse.2006.09.026, 2007.

Qian, Y., Flanner, M. G., Leung, L. R., and Wang, W.: Sensitivity studies on the impacts of Tibetan Plateau snowpack pollution on the Asian hydrological cycle and monsoon climate, Atmos. Chem. Phys., 11, 1929–1948, doi: 10.5194/acp-11-1929-2011, 2011.

Qian, Y., Yasunari, T. J., Doherty, S. J., Flanner, M. G., Lau, W. K. M., Ming, J., Wang, H., Wang, M., Warren, S. G., and Zhang, R.: Light-absorbing particles in snow and ice: Measurement and modeling of climatic and hydrological impact, Adv. Atmos. Sci., 32, 64–91, doi: 10.1007/s00376-014-0010-0, 2015.

Qiu, J.: China: The third pole, Nature, 454, 393–396, doi: 10.1038/454393a, 2008.

Ramanathan, V., Ramana, M. V., Roberts, G., Kim, D., Corrigan, C., Chung, C., and Winker, D.: Warming trends in Asia amplified by brown cloud solar absorption, Nature, 448, 575–578, doi: 10.1038/nature06019, 2007.

Ramanathan, V. and Carmichael, G.: Global and regional climate changes due to black carbon, Nature Geosci, 1, 221–227, doi: 10.1038/ngeo156, 2008.

Seaman, N. L., Stauffer, D. R., and Lario-Gibbs, A. M.: A Multiscale Four-Dimensional Data Assimilation System Applied in the San Joaquin Valley during SARMAP. Part I: Modeling Design and Basic Performance Characteristics, J. Appl. Meteor., 34, 1739–1761, doi: 10.1175/1520-0450(1995)034<1739:AMFDDA>2.0.CO;2, 1995.

Singh, P. and Bengtsson, L.: Hydrological sensitivity of a large Himalayan basin to climate change, Hydrol. Process., 18, 2363–2385, doi: 10.1002/hyp.1468, 2004.

Skamarock, W. C., Klemp, J. B., Dudhia, J., Gill, D. O., Barker, D. M., Duda, M. G., Huang, X., Wang, W., and Powers, J. G.: A description of the advanced research WRF version 3, NCAR Tech. Note, NCAR/TN-475+STR,, Natl. Cent. for Atmos. Res., Boulder, CO, USA, 8 pp. available online at: http://www.mmm.ucar.edu/wrf/users/docs/arw v3.pdf, 2008.

Stauffer, D. R. and Seaman, N. L.: Use of Four-Dimensional Data Assimilation in a Limited-Area Mesoscale Model. Part I: Experiments with Synoptic-Scale Data, Mon. Wea.

https://doi.org/10.5194/acp-2019-905
Preprint. Discussion started: 14 October 2019

Rev., 118, 1250–1277, doi: 10.1175/1520-0493(1990)118<1250:UOFDDA>2.0.CO;2, 1990.

Vernekar, K. G., Sinha, S., Sadani, L. K., Sivaramakrishnan, S., Parasnis, S. S., Mohan, B., Dharmaraj, S., Patil, M. N., Pillai, J. S., and Murthy, B. S.: An overview of the land surface processes experiment (LASPEX) over a semi-arid region of India, Boundary-layer meteorology, 106, 561–572, 2003.

Wang, X., Gong, P., Sheng, J., Joswiak, D. R., and Yao, T.: Long-range atmospheric transport of particulate Polycyclic Aromatic Hydrocarbons and the incursion of aerosols to the southeast Tibetan Plateau, Atmospheric Environment, 115, 124–131, doi: 10.1016/j.atmosenv.2015.04.050, 2015.

Wiedinmyer, C., Akagi, S. K., Yokelson, R. J., Emmons, L. K., Al-Saadi, J. A., Orlando, J. J., and Soja, A. J.: The Fire INventory from NCAR (FINN): a high resolution global model to estimate the emissions from open burning, Geosci. Model Dev., 4, 625–641, doi: 10.5194/gmd-4-625-2011, 2011.

Wu, G. X., Liu, Y. M., Liu, X., Duan, A. M., and Liang, X. Y.: How the heating over the Tibetan Plateau affects the Asian climate in summer, Chinese J. Atmos. Sci, 29, 47–56, 2005.

Wu, G., Liu, Y., Dong, B., Liang, X., Duan, A., Bao, Q., and Yu, J.: Revisiting Asian monsoon formation and change associated with Tibetan Plateau forcing: I. Formation, Clim Dyn, 39, 1169–1181, doi: 10.1007/s00382-012-1334-z, 2012.

Wu, G., Duan, A., and Liu, Y.: Atmospheric Heating Source Over the Tibetan Plateau and Its Regional Climate Impact, Oxford Research Encyclopedia of Climate Science, doi: 10.1093/acrefore/9780190228620.013.588, 2019.

Xia, X., Zong, X., Cong, Z., Chen, H., Kang, S., and Wang, P.: Baseline continental aerosol over the central Tibetan plateau and a case study of aerosol transport from South Asia, Atmospheric Environment, 45, 7370–7378, doi: 10.1016/j.atmosenv.2011.07.067, 2011.

Xu, B., Cao, J., Hansen, J., Yao, T., Joswia, D. R., Wang, N., Wu, G., Wang, M., Zhao, H., Yang, W., Liu, X., and He, J.: Black soot and the survival of Tibetan glaciers, PNAS, 106, 22114–22118, doi: 10.1073/pnas.0910444106, 2009.

Yang, J., Kang, S., Ji, Z., and Chen, D.: Modeling the Origin of Anthropogenic Black Carbon and Its Climatic Effect Over the Tibetan Plateau and Surrounding Regions, J. Geophys. Res. Atmos., 123, 671–692, doi: 10.1002/2017JD027282, 2018.

Yasunari, T. J., Bonasoni, P., Laj, P., Fujita, K., Vuillermoz, E., Marinoni, A., Cristofanelli, P., Duchi, R., Tartari, G., and Lau, K.-M.: Estimated impact of black carbon deposition

https://doi.org/10.5194/acp-2019-905
Preprint. Discussion started: 14 October 2019

during pre-monsoon season from Nepal Climate Observatory – Pyramid data and snow albedo changes over Himalayan glaciers, Atmos. Chem. Phys., 10, 6603–6615, doi: 10.5194/acp-10-6603-2010, 2010.

Ye, D.-Z. and Wu, G.-X.: The role of the heat source of the Tibetan Plateau in the general circulation, Meteorl. Atmos. Phys., 67, 181–198, doi: 10.1007/BF01277509, 1998.

Zaveri, R. A. and Peters, L. K.: A new lumped structure photochemical mechanism for large-scale applications, J. Geophys. Res., 104, 30387–30415, doi: 10.1029/1999JD900876, 1999.

Zaveri, R. A., Easter, R. C., Fast, J. D., and Peters, L. K.: Model for simulating aerosol interactions and chemistry (MOSAIC), J. Geophys. Res. Atmos., 113, 2008.

Zhang, Aoqi, Yunfei Fu, Yilun Chen, Guosheng Liu and Xiangdong Zhang: Impact of the surface wind flow on precipitation characteristics over the southern Himalayas: GPM observations, Atmospheric Research, 202, (10), (2018).

Zhang, R., Wang, H., Qian, Y., Rasch, P. J., Easter, R. C., Ma, P.-L., Singh, B., Huang, J., and Fu, Q.: Quantifying sources, transport, deposition, and radiative forcing of black carbon over the Himalayas and Tibetan Plateau, Atmos. Chem. Phys., 15, 6205–6223, doi: 10.5194/acp-15-6205-2015, 2015.

Zhang, R., Wang, Y., He, Q., Chen, L., Zhang, Y., Qu, H., Smeltzer, C., Li, J., Alvarado, L. M. A., Vrekoussis, M., Richter, A., Wittrock, F., and Burrows, J. P.: Enhanced trans-Himalaya pollution transport to the Tibetan Plateau by cut-off low systems, Atmos. Chem. Phys., 17, 3083–3095, doi: 10.5194/acp-17-3083-2017, 2017.

Zhao, C., Liu, X., Leung, L. R., Johnson, B., McFarlane, S. A., Gustafson, W. I., Fast, J. D., and Easter, R.: The spatial distribution of mineral dust and its shortwave radiative forcing over North Africa: modeling sensitivities to dust emissions and aerosol size treatments, Atmos. Chem. Phys., 10, 8821–8838, doi: 10.5194/acp-10-8821-2010, 2010.

Zhao, C., Liu, X., Leung, L. R., and Hagos, S.: Radiative impact of mineral dust on monsoon precipitation variability over West Africa, Atmos. Chem. Phys., 11, 1879-1893, doi: 10.5194/acp-11-1879-2011, 2011.

Zhao, C., Ruby Leung, L., Easter, R., Hand, J., and Avise, J.: Characterization of speciated aerosol direct radiative forcing over California, J. Geophys. Res. Atmos., 118, 2372–2388, doi: 10.1029/2012JD018364, 2013(a).

Zhao, C., Chen, S., Leung, L. R., Qian, Y., Kok, J., Zaveri, R., and Huang, J.: Uncertainty in modeling dust mass balance and radiative forcing from size parameterization, Atmos. Chem. Phys., 13, 10733–10753, doi: doi:10.5194/acp-13-10733-2013, 2013(b).

Zhao, C., Hu, Z., Qian, Y., Leung, L. R., Huang, J., Huang, M., Jin, J., Flanner, M., Zhang, R., Wang, H., Yan, H., Lu, Z., and Streets, D. G.: Simulating black carbon and dust and their radiative forcing in seasonal snow: a case study over North China with field campaign measurements, Atmos. Chem. Phys., 14, 11475–11491, doi: doi:10.5194/acp-14-11475-2014, 2014.

Zhao, C., Huang, M., Fast, J. D., Berg, L. K., Qian, Y., Guenther, A., Gu, D., Shrivastava, M., Liu, Y., and Walters, S.: Sensitivity of biogenic volatile organic compounds to land surface parameterizations and vegetation distributions in California, Geosci. Model Dev, 9, 1959–1976, doi: 10.5194/gmd-9-1959-2016, 2016.

Zhao, P., Zhou, X., Chen, J., Liu, G., and Nan, S.: Global climate effects of summer Tibetan Plateau, Science Bulletin, 64, 1–3, doi: 10.1016/j.scib.2018.11.019, 2019.

Zhao, Z., Cao, J., Shen, Z., Xu, B., Zhu, C., Chen, L.-W. A., Su, X., Liu, S., Han, Y., Wang, G., and Ho, K.: Aerosol particles at a high-altitude site on the Southeast Tibetan Plateau, China: Implications for pollution transport from South Asia, J. Geophys. Res. Atmos., 118, 11,360-11,375, doi: 10.1002/jgrd.50599, 2013.

Zhang, Y. L., S. Kang, Z. Cong, J. Schmale, M. Sprenger, C. Li, W. Yang, T. Gao, M. Sillanpää, X. Li, Y. Liu, P. Chen, X. Zhang: Light-absorbing impurities enhance glacier albedo reduction in the southeastern Tibetan Plateau. Journal of Geophysical Research - Atmosphere, 122. Doi: 10.1002/2016JD026397, 2017.

Zhang, Y. L., S. Kang, M. Sprenger, Z. Cong, T. Gao, C. Li, S. Tao, X. Li, X. Zhong, M. Xu, W. Meng, B. Neupane, X. Qin, M. Sillanpää: Black carbon and mineral dust in snow cover on the Tibetan Plateau. The Cryosphere, 12: 413-431. Doi: 10.5194/tc-12-413-2018, 2018.

https://doi.org/10.5194/acp-2019-905
Preprint. Discussion started: 14 October 2019

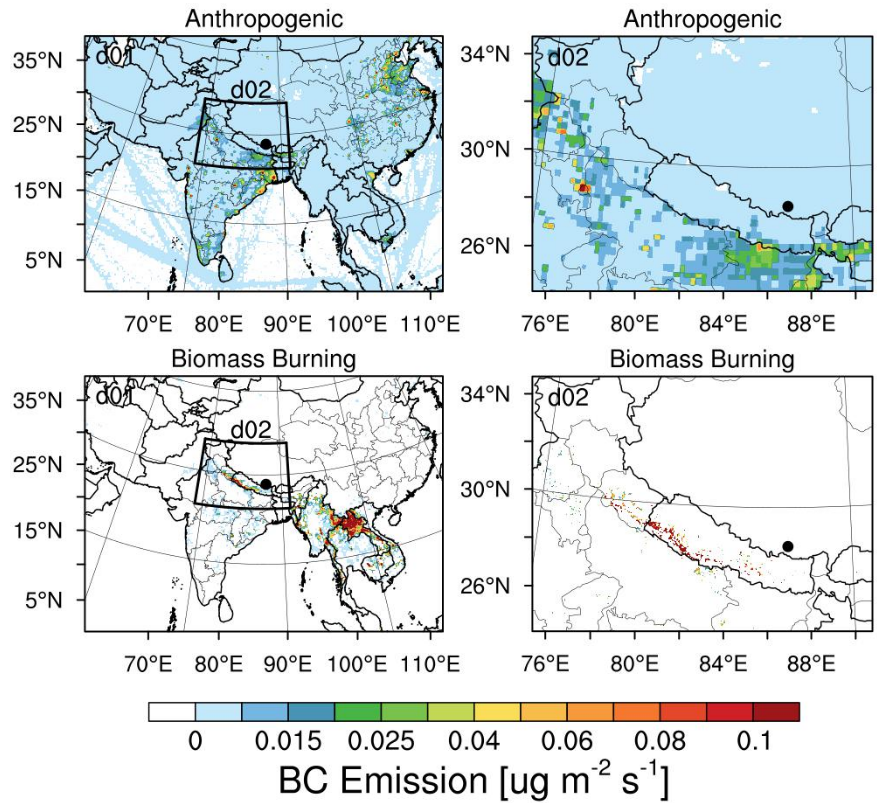

Figure 1. Anthropogenic and fire emissions over the entire simulated regions of 20 km and 4 km resolutions, the dot represents the Everest Observation Site (QOMS).

https://doi.org/10.5194/acp-2019-905
Preprint. Discussion started: 14 October 2019

Atmospheric Chemistry and Physics
Discussions

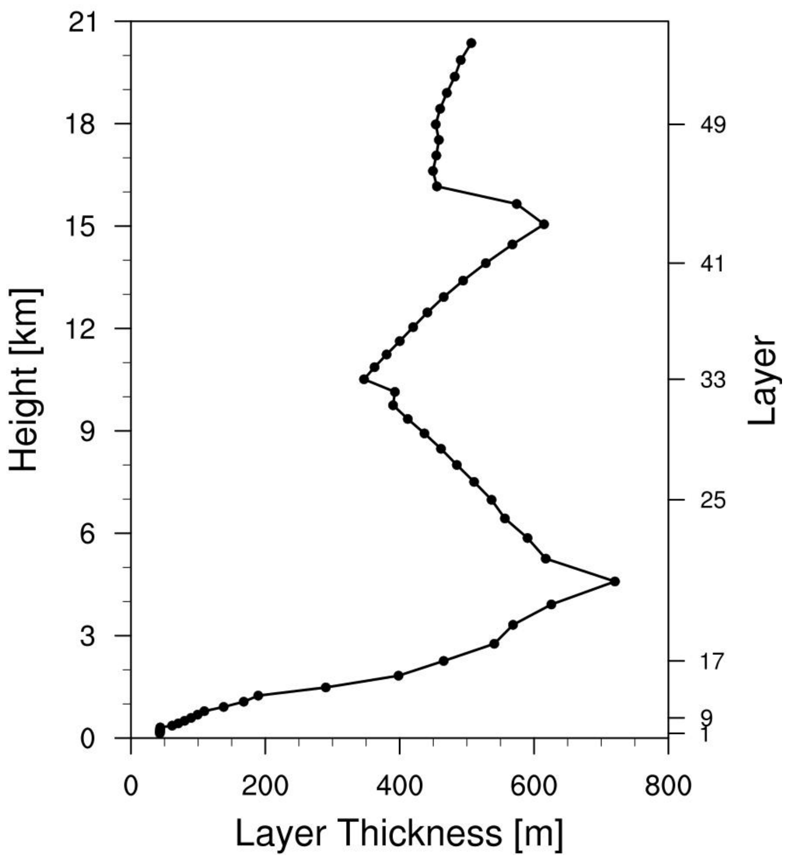

Figure 2. The thickness of each vertical layer in the simulations (54 layers in total).

https://doi.org/10.5194/acp-2019-905
Preprint. Discussion started: 14 October 2019

Atmospheric Chemistry and Physics
Discussions
Open Access

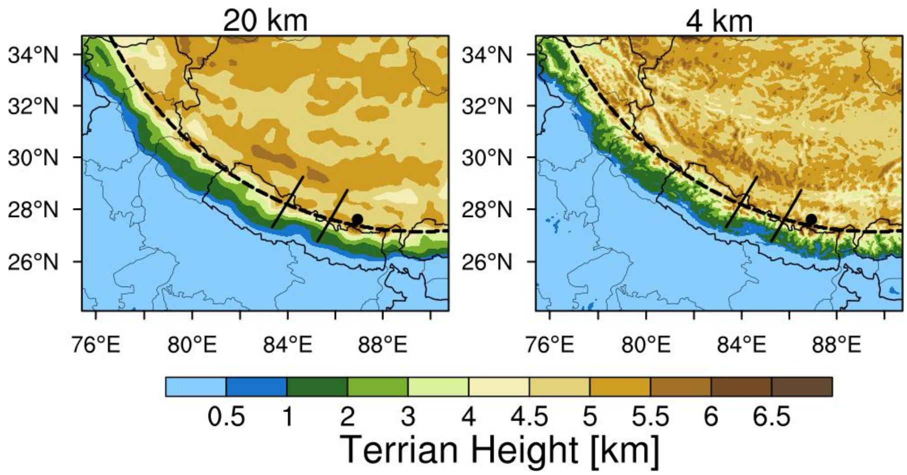

Figure 3. Spatial distributions of terrain height from the simulations at 20 km and 4 km resolutions. The two black lines and one dash line represent the cross sections for analysis in the following.

https://doi.org/10.5194/acp-2019-905
Preprint. Discussion started: 14 October 2019

Atmospheric Chemistry and Physics
Discussions

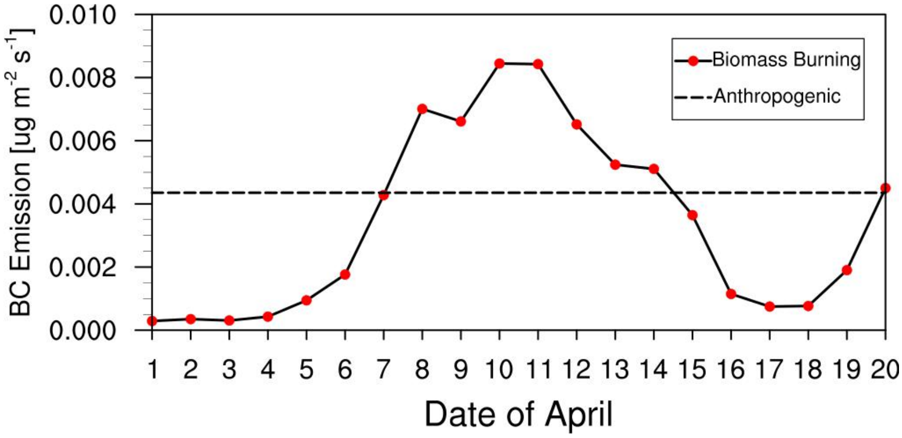

Figure 4. Time series of area-averaged daily fire emissions between 26°N and 29°N over the simulation domain at 4 km resolution (The dash line in the figure represents the anthropogenic emission).

https://doi.org/10.5194/acp-2019-905
Preprint. Discussion started: 14 October 2019

Atmospheric Chemistry and Physics
Discussions

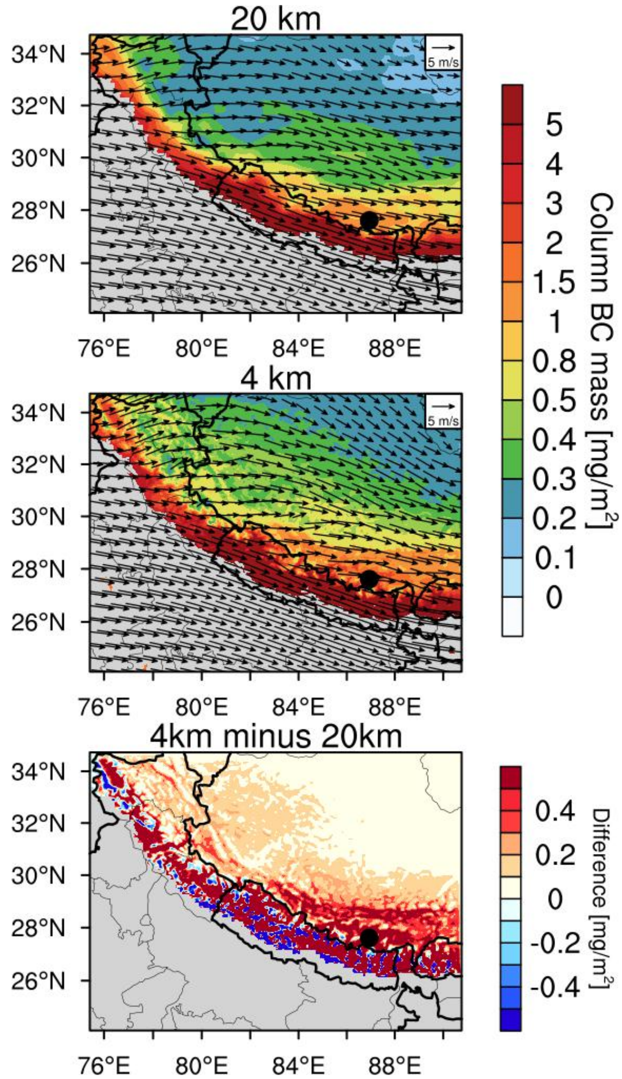

Figure 5. Column integrated BC mass in the area with the terrain height larger than 0.5 km and the wind fields at 500 hPa from the simulations at 20 km and 4 km horizontal resolutions averaged for April 5-20, 2016. The difference between the simulations at 4 km and 20 km resolutions is also shown.

https://doi.org/10.5194/acp-2019-905
Preprint. Discussion started: 14 October 2019

Atmospheric Chemistry and Physics
Discussions

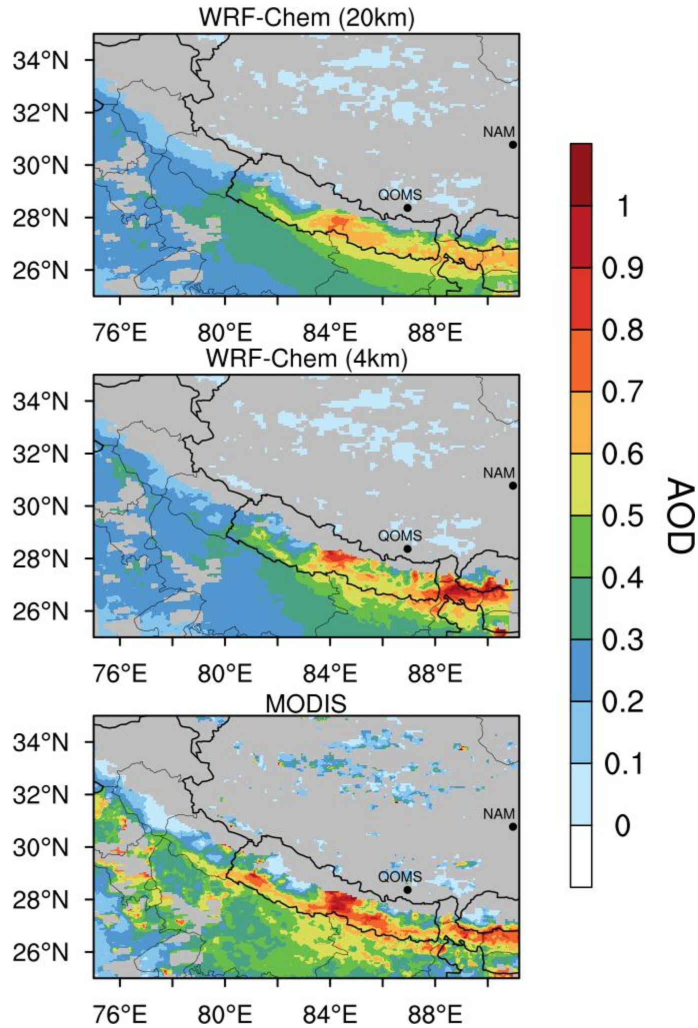

Figure 6. Spatial distributions of AOD from the MODIS retrievals and the simulations at 4 km and 20 km resolutions averaged for April 5-20, 2016. The two black dots represent the two AERONET sites over the TP (QOMS, 86.56°E, 28.21°N; NAM, 90.96°E, 30.77°N).

https://doi.org/10.5194/acp-2019-905
Preprint. Discussion started: 14 October 2019

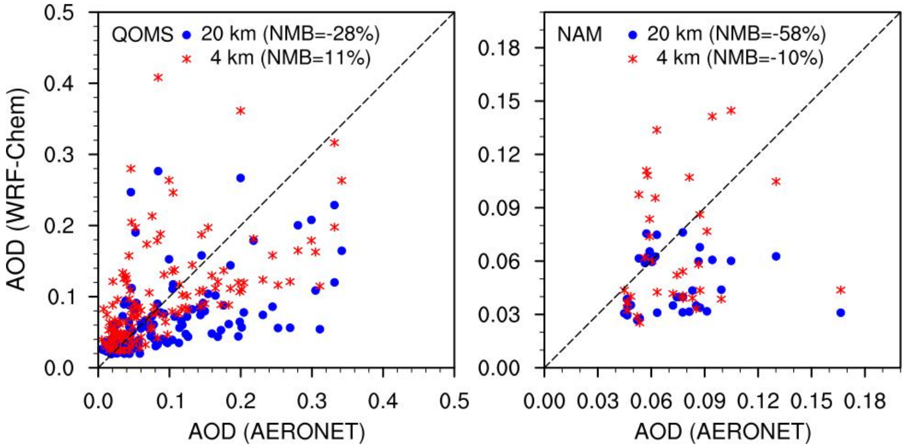

Figure 7. Hourly AOD from the measurements of AERONET and simulations by WRF-Chem at the two sites over the TP (QOMS, 86.56°E, 28.21°N; NAM, 90.96°E, 30.77°N) for April, 2016.

https://doi.org/10.5194/acp-2019-905
Preprint. Discussion started: 14 October 2019

Atmospheric Chemistry and Physics
Discussions

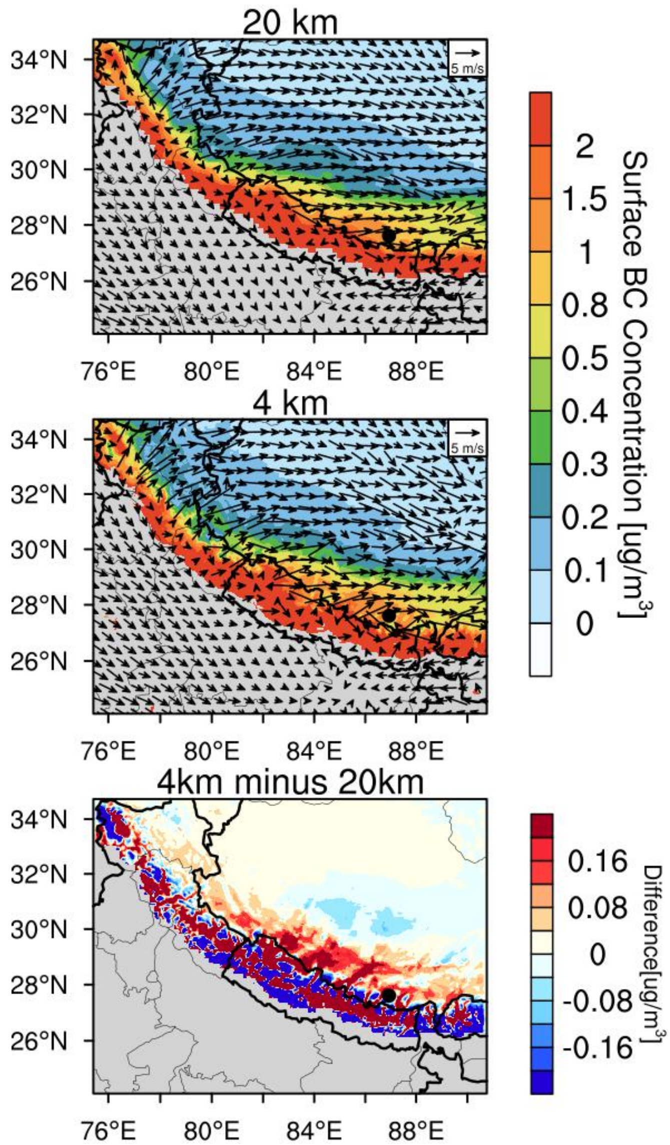

Figure 8. Spatial distributions of surface BC concentration and surface wind field over the inner domain from the simulations at 4 km and 20 km resolutions. The difference between the simulations at 4 km and 20 km resolutions is also shown.

https://doi.org/10.5194/acp-2019-905
Preprint. Discussion started: 14 October 2019

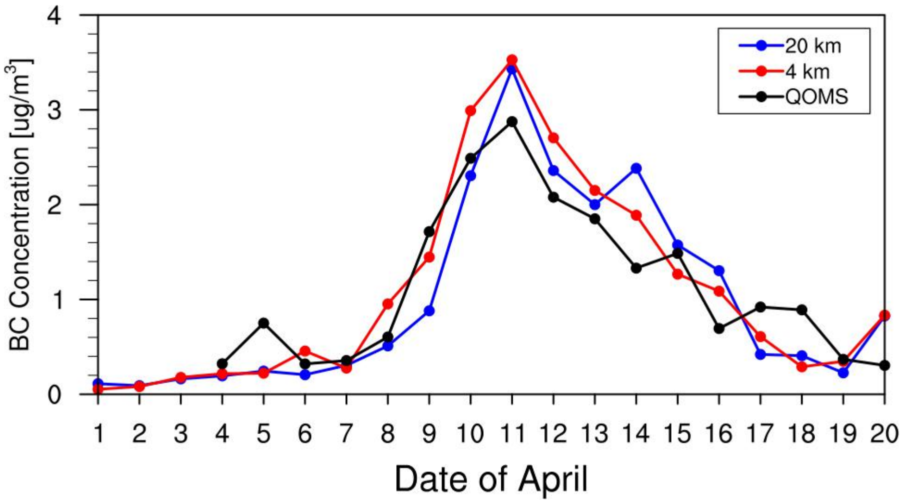

Figure 9. The simulated (colored) and observed (black) temporal variability of surface BC mass concentration at the measurement site during April 1-20 in 2016.

https://doi.org/10.5194/acp-2019-905
Preprint. Discussion started: 14 October 2019

Atmospheric Chemistry and Physics
Discussions

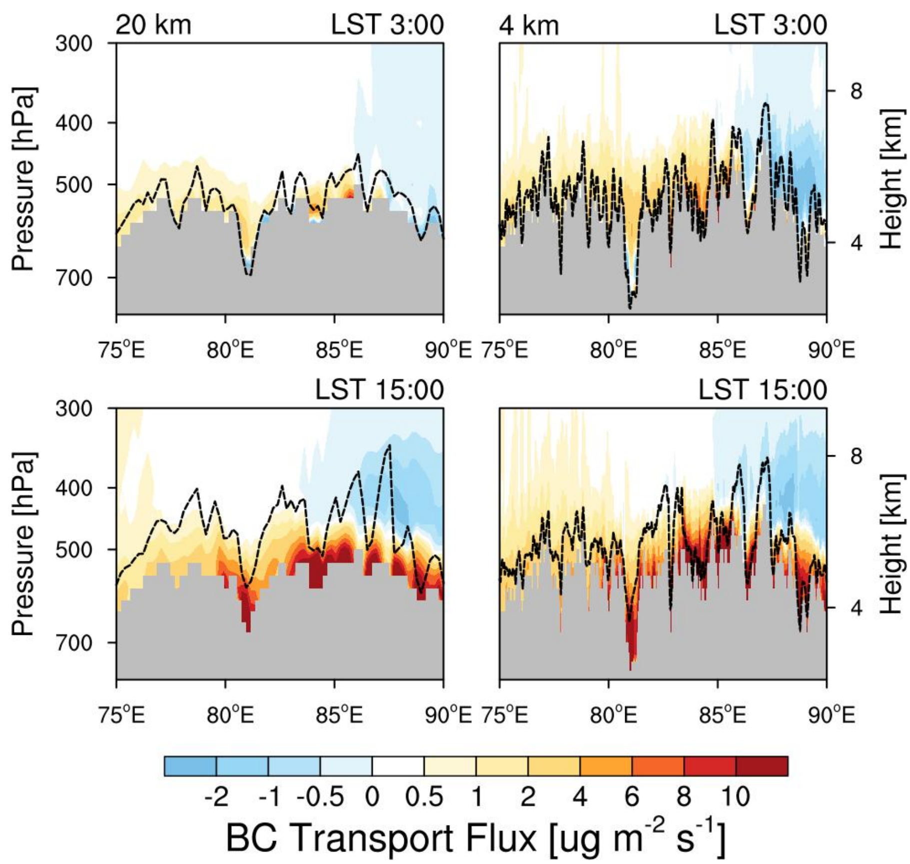

Figure 10. Longitude-height cross section of BC transport flux along the cross line (shown as the black dash line in Fig. 3) from the simulations at 20 km and 4 km resolutions at local time (LT) 03:00 and 15:00 averaged for April 5-20. The PBL height along the cross section is shown here as the black dash line.

Atmospheric Chemistry and Physics
Discussions

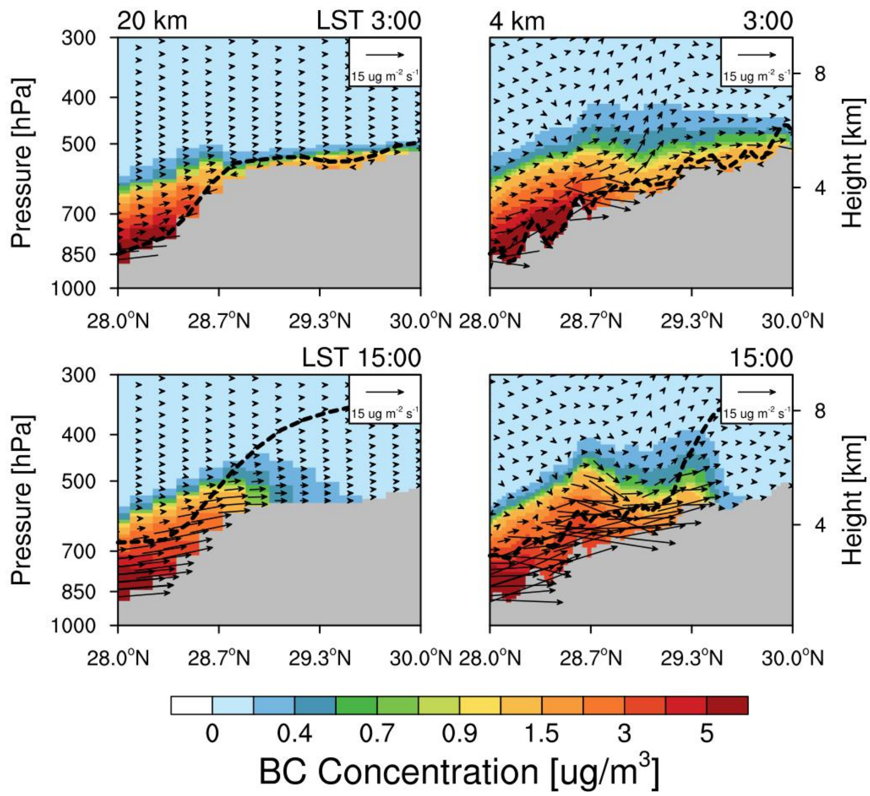

Figure 11. Latitude-height cross section of BC flux (vector) along the valley (shown as the black line in Fig. 3) from the simulations at 20 km and 4 km resolutions at local time (LT) 03:00 and 15:00 averaged for April 5-20, 2016. Contour represents the BC concentration.

https://doi.org/10.5194/acp-2019-905
Preprint. Discussion started: 14 October 2019

Atmospheric Chemistry and Physics
Discussions

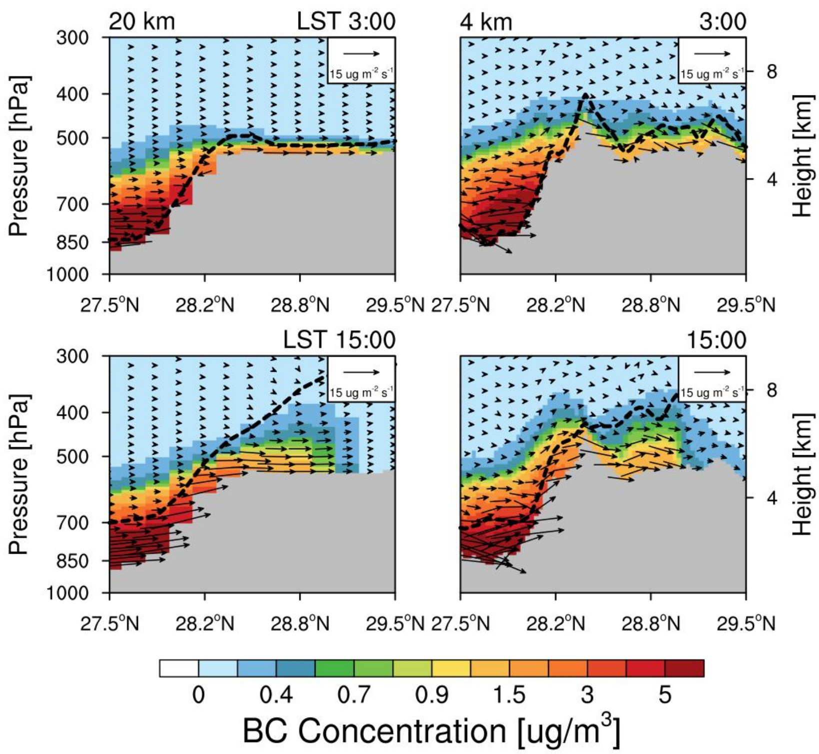

Figure 12. Latitude-height cross section of BC flux (vector) across the mountain (shown as the black line in Fig. 3) from the simulations at 20 km and 4 km resolutions at local time (LT) 03:00 and 15:00 averaged for April 5-20, 2016. Contour represents the BC concentration.

https://doi.org/10.5194/acp-2019-905
Preprint. Discussion started: 14 October 2019

Atmospheric Chemistry and Physics
Discussions

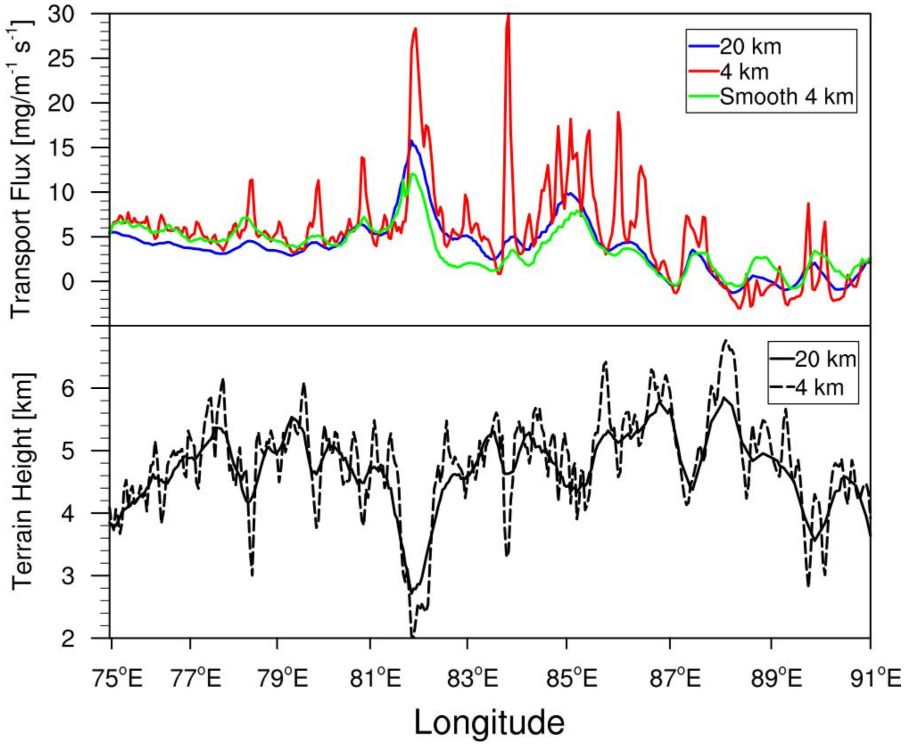

Figure 13. Longitudinal distribution of integrated BC mass fluxes along the cross section in Fig. 10 from the simulations at 20 km and 4 km resolutions. The result (Smooth 4 km) from the sensitivity experiment at 4 km resolution but with the smoothing 20km-resolution topography is also shown. The black lines represent the terrain heights along the cross section at 20 km and 4 km resolutions.

https://doi.org/10.5194/acp-2019-905
Preprint. Discussion started: 14 October 2019

Atmospheric Chemistry and Physics Discussions

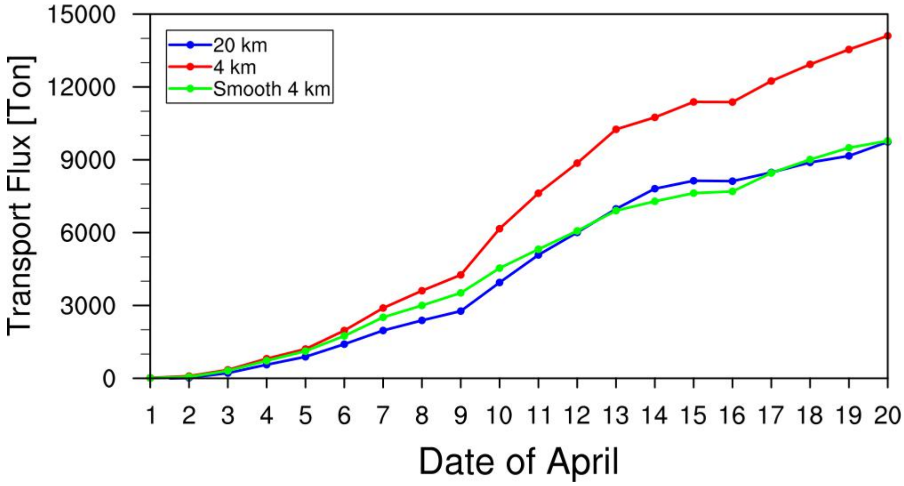

Figure 14. Accumulated integrated total transport flux of BC across the Himalayas estimated from the simulations at 20 km and 4 km resolutions during April 1-20, 2016. The sensitivity experiment at 4 km resolution but with the smoothing 20km-topography is also shown.

https://doi.org/10.5194/acp-2019-905
Preprint. Discussion started: 14 October 2019

Atmospheric Chemistry and Physics
Discussions

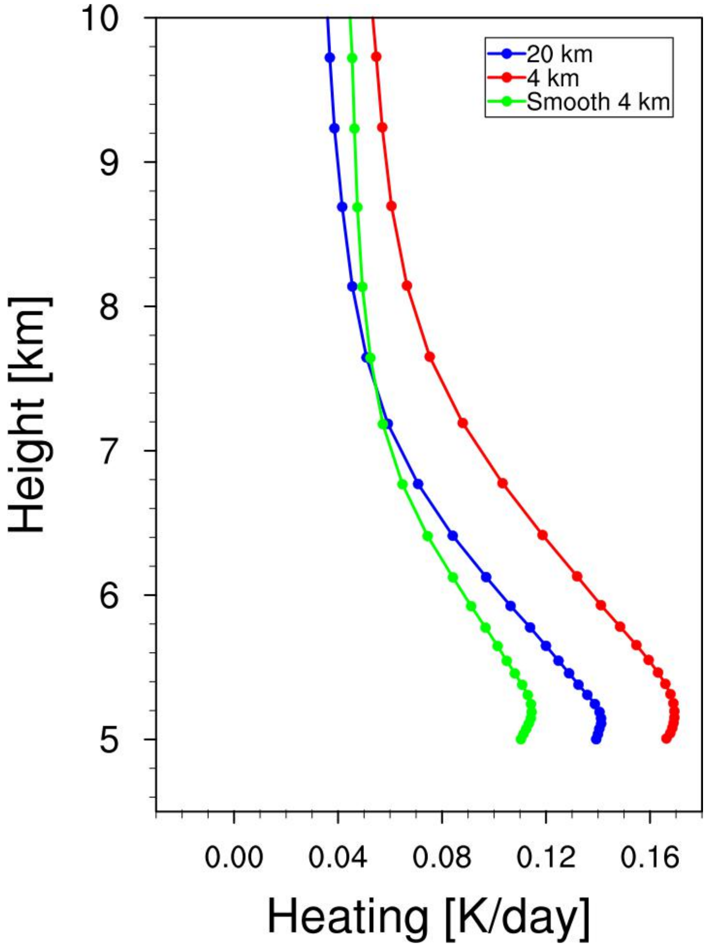

Figure 15. Vertical profiles of BC induced radiative heating rates in the atmosphere averaged over the TP (with elevation > 4 km) within the inner domain shown in Fig. 1 from the simulations at 20 km and 4 km resolutions during April 5-20, 2016. The sensitivity experiment at 4 km resolution but with the smoothing 20 km-topography is also shown.

https://doi.org/10.5194/acp-2019-905
Preprint. Discussion started: 14 October 2019

Atmospheric Chemistry and Physics
Discussions

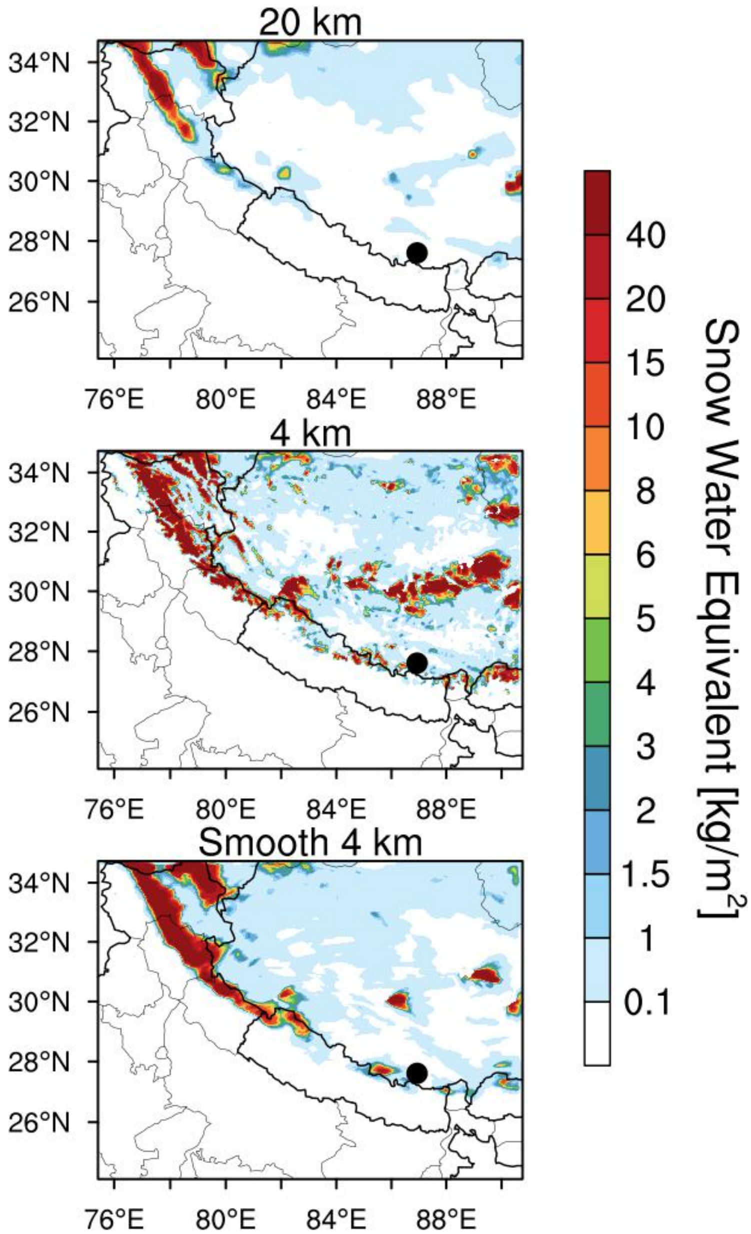

Figure 16. Spatial distributions of snow water equivalent averaged for April 5-20, 2016 from the simulations at 20 km and 4 km resolutions. The sensitivity experiment at 4 km resolution but with the smoothing 20km-topography is also shown.

https://doi.org/10.5194/acp-2019-905
Preprint. Discussion started: 14 October 2019

Atmospheric Chemistry and Physics
Discussions

1355
1356

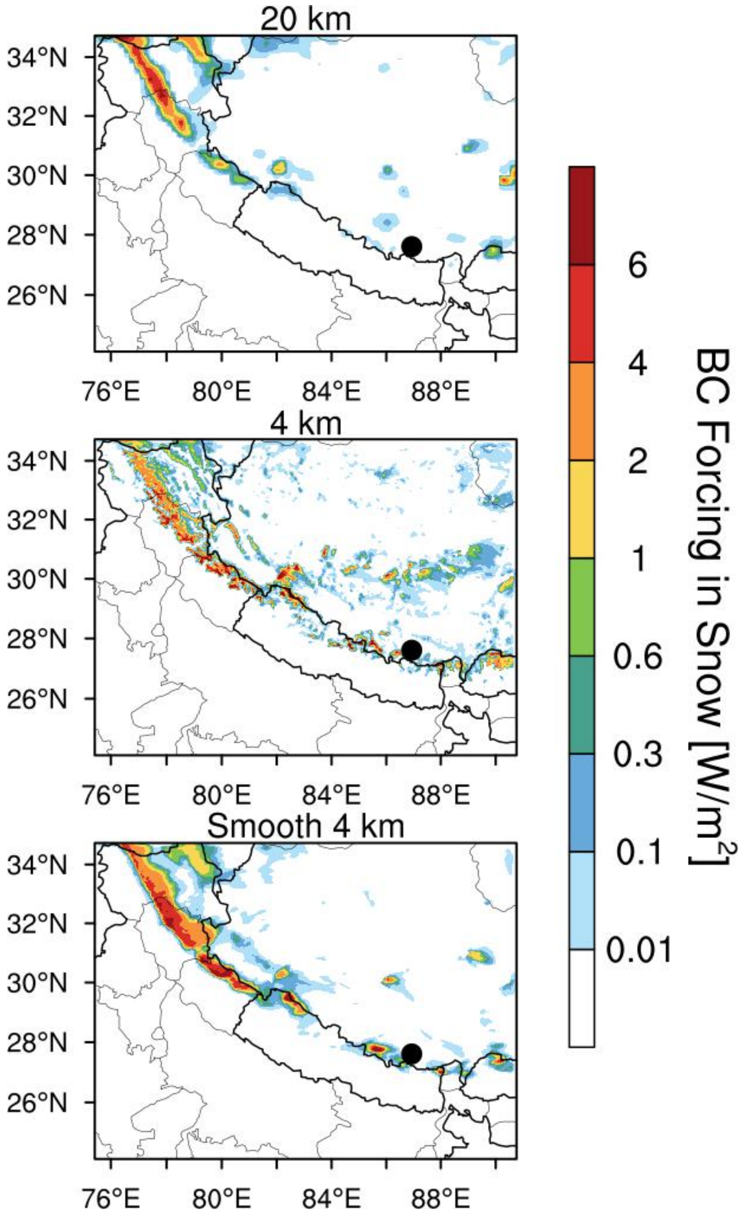

1357
1358
1359 **Figure 17.** Spatial distributions of BC radiative forcing in the surface snow averaged for
1360 April 5-20, 2016 from the simulations at 20 km and 4 km resolutions. The sensitivity
1361 experiment at 4 km resolution but with the smoothing 20km-topography is also shown.
1362